Referee 1

This paper presents the measurements of OH, HO2, and RO2 radicals and OH reactivity in central Beijing in the summer of 2017 as part of the APHH campaign. It reportes the highest ever observed OH concentration of 2.8×107 cm-3 in urban area, even slightly higher than that reported in PRD in China by Lu et al. (2012).

Experimental budget analysis of OH, HO2, RO2, and ROx was performed in the similar way as Tan et al. (2019) did in PRD in 2014. Consistent with other studies in China, the authors found a missing OH source under low NO (<0.5 ppbv) and high VOC condition. Besides, the authors found the opposite trends in HO2 budget and RO2 budget. The HO2 production rate exceeded the destruction rate by the similar rate as the RO2 destruction rate exceed production rate. The authors explained the opposite difference as the substantially slower than assumed net propagation rate of RO2 to HO2. If only 10% of the RO2 radicals propagate to HO2 upon reaction with NO, the HO2 and RO2 budget would be closed. The authors also performed a model simulation based on MCM 3.3.1, and found consistent results with the experimental budget analysis, except for the OH radical. The model simulated OH concentration very well due to a cancellation of missing OH source and sinks terms in its budget. The model underpredicted the kOH consistently across all NOx levels. To understand the model biases, the authors performed several sensitivity tests. The inclusion of heterogeneous loss of HO2 to aerosol surfaces and ClNO2 chemistry could not entirely explained the HO2 overestimation and RO2 underestimation, respectively. Several sensitivity tests were done to see the impact of missing OH reactivity on the modelled radical concentrations by assuming reactants convert OH to CH3O2, OHCH2CHO2O2, CH3(O)O2, and C96O2. The authors proposed that missing OH reactivity converted OH to a larger RO2 that undergo several reaction with NO, before eventually generating HO2, could improve the agreement between observation and simulation, and they used an α-pinene-derived RO2 species (C96O2) as an example. The results are of interest to the atmospheric chemistry community, enriching the ROx measurement in megacity, and the paper is worthy of publication. However, there are some critical issues and mistakes have to be addressed and corrected in advance before publication. Also, the paper could be shortened quite a bit and the writing could be more concisely and logically.

We thank referee 1 for their useful comments and have responded to each specific comment in bold below. The changes to the manuscript that we will make are in red.

1. Line 337, Alkyl nitrates are not formed from aldehydes + NO3.

This was a typo and should have been:

Alkyl nitrates, formed from isoprene + NO3 were also enhanced at these times at this site (Reeves et al., 2019).

This will be corrected in the revised manuscript

2. According to the Fig.4, the RO2 neutral reaction rate (RO2+NO->RO2) has no dependence towards NO concentration since the P:D(HO2) showed no tendency towards lower NO. However, as the NO decreased, the competitive reaction of RO2 with HO2 or RO2 isomerization would become more and more important, and was even comparable to the rate between RO2 and NO. Thus, the multiple conversion of one RO2 to another should be reduced towards low NO.

In response to a comment from the second reviewer, we have added model scenario 'Missing k(OH) (OH to C96O2)' to part of the radical measurement time-series, alongside the base model scenario to highlight that additional VOC reactivity which produces RO_2 radicals that isomerise after reaction with NO is able to increase the modelled total RO_2 concentration both under the lower NO conditions experienced between the 16th – 22nd June as well as on the higher NO days 9th – 12th June indicating that NO is still at sufficient concentrations to dominate the fate of RO_2 between the 16th – 22nd June, despite NO concentrations being lower.

However, as the referee states, in the afternoon low-NO chemistry (e.g. RO_2+HO_2 reactions) does play a greater role (30%), see Newland et al., (2020). Under these conditions, the reaction of RO_2 with NO and, therefore, the subsequent RO isomerisation, becomes less efficient and this trend is demonstrated when we overlay the RO_2 median measured to modelled (Missing k(OH) (OH to C96O2)) ratio vs NO on figure S3. We hypothesise that the production rate of HO_2 exceeds the destruction rate of HO_2 by a similar amount across the whole NO range encountered because we are neglecting both RO_2+NO reactions that lead to an RO radical that is able to undergo isomerisation reactions which would serve to reduce alpha most strongly under high NO conditions, whilst under low NO conditions we are neglecting RO_2 unimolecular reactions which may form OH directly rather than HO_2.

Newland, M. J., Bryant, D. J., Dunmore, R., Bannan, T., Acton, W. J., Langford, B., Hopkins, J., Squires, F. A., Dixon, W. J., Drysdale, W. S., Ivatt, P. D., Evans, M. J., Edwards, P., Whalley, L. K., Heard, D. E., Slater, E. J., Woodward-Massey, R., Ye, C., Mehra, A., Worrall, S. D., Bacak, A., Coe, H., Percival, C., Hewitt, C. N., Lee, J. D., Cui, T. Q., Surratt, J. D., Wang, X., Lewis, A. C., Rickard, A. R., and Hamilton, J.: Rainforest-like atmospheric chemistry in a polluted megacity, Atmospheric Chemistry and Physics Discussions, 35, 2020.

Pg 14, line 440 onwards: The model under-estimates total RO_2 throughout the measurement period, although the level of disagreement (in absolute concentration) is most severe from the 16th – 22nd June when NO concentrations were at their lowest. During this period, the average NO mixing ratio was ~0.4 ppbv during the afternoon hours, whilst the average NO mixing ratio for the entirety of the campaign was ~0.75 ppbv during the afternoons (Fig S1 in SI). The average peak NO mixing ratio observed in the morning between 16th – 22nd June was just over 6 ppbv, whilst the average peak NO mixing ratio for the entirety of the campaign was close to 16 ppbv.

Pg 18, line 566 onwards: The modelled radical concentrations predicted from the 'Missing k(OH) (OH to C96O2)' scenario are overlaid with the radical observations and modelled radicals from the base model scenario in Fig S2, SI. The additional VOC reactivity which produces RO_2 radicals that isomerise after reaction with NO is able to increase the modelled total RO_2 concentration both under the lower NO conditions experienced between the 16th – 22nd June as well as on the higher NO days 9th – 12th June indicating that NO is still at sufficient concentrations to dominate the fate of RO_2 between the 16th – 22nd June, despite NO concentrations being lower. The median measured to modelled (Missing k(OH) (OH to C96O2)) ratio vs NO (Fig S3, SI) highlights that the inclusion of alkoxy isomerisation following RO_2 + NO reaction increases the modelled RO_2 across the entire NO range but, considering the log scale, has the biggest impact on the ratio (from the measured to modelled (base) ratio) at the highest NO concentration. Both the simple- and complex-RO_2 species are enhanced, as the

first 3 generations of RO_2 species formed would be detected during the RO_x-mode in the RO_x-LIF instrument and, hence, contribute to RO_2-simple.

Supplementary Information

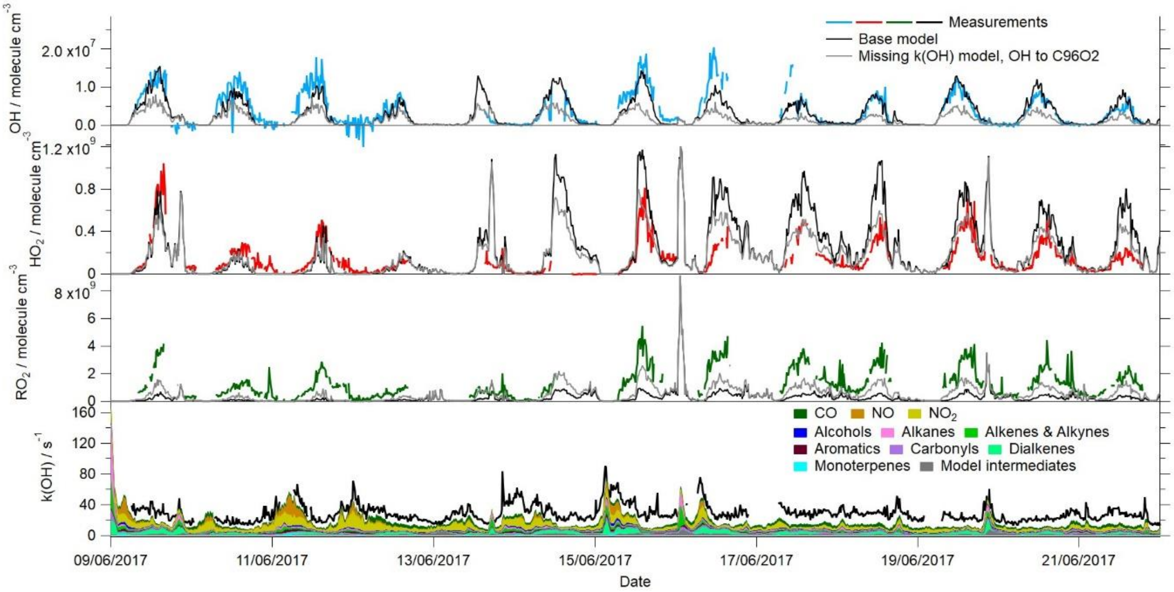

Figure S2: Time-series of the measured and modelled OH, HO_2, total RO_2 and OH reactivity from the 9th – 22nd June which encompasses high NO days (9th – 12th June) and low NO days (16th – 22nd June).

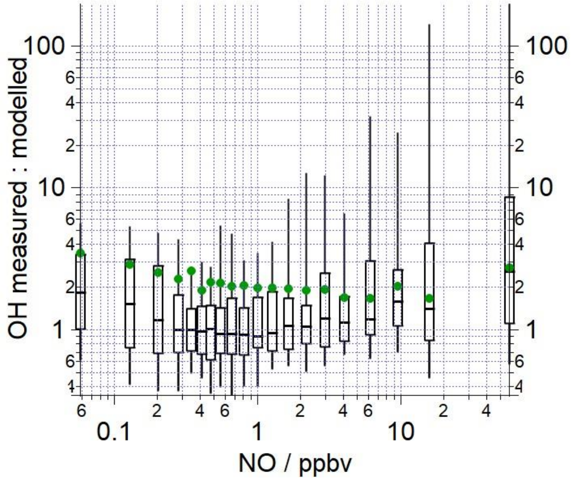

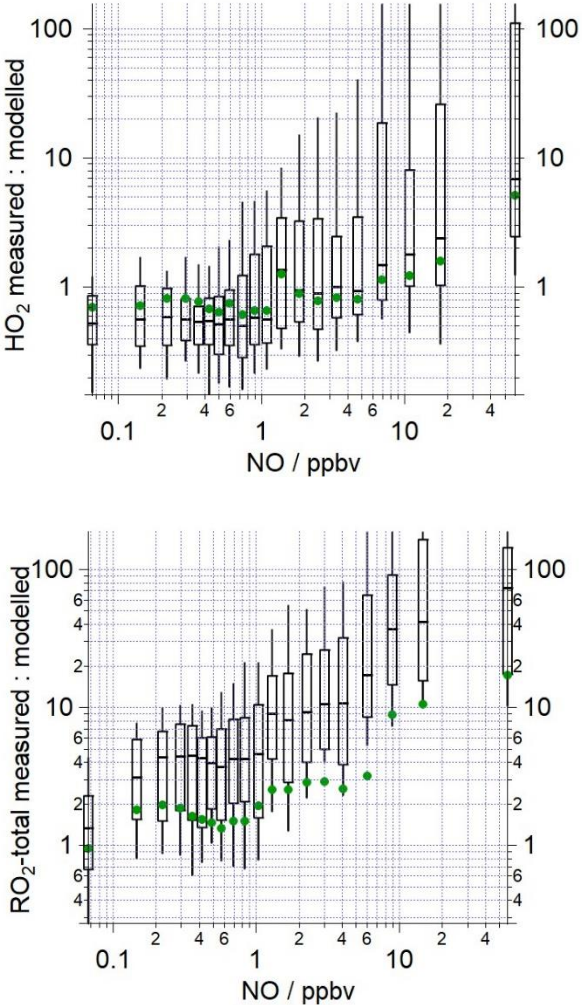

Figure S3: The median ratio (-) of the measured to modelled (base) OH, HO$_2$ and total RO$_2$ binned over the NO mixing ratio range encountered during the campaign on a logarithmic scale. The box and whiskers represent the 25th/75th and 5th/95th confidence intervals. The green circles display the measured to modelled OH, HO$_2$ and total RO$_2$ ratio when the model includes missing OH reactivity in the form of a single reaction which converts OH to C96O2. The number of data points in each of the NO bins is ~80

The median measured to modelled (Missing k(OH) (OH to C96O2)) ratio vs NO (green circles) is displayed in figure S3 alongside median measured to modelled (base) ratio. The inclusion of alkoxy isomerisation following RO$_2$ + NO reaction increases the modelled RO$_2$ concentration across the entire NO range but, considering the log scale, has the biggest impact on the ratio (from the measured to modelled (base) ratio) at the highest NO concentration. The HO$_2$ median measured to modelled (Missing k(OH) (OH to C96O2)) ratio vs NO in the middle panel increases from the measured to modelled (base) ratio at NO mixing ratios <1 ppbv, indicating improved

agreement. At higher NO mixing ratios, where the base model begins to underpredict HO_2, due to the large under-prediction in RO_2, this under-prediction is reduced in the missing k(OH) (OH to C96O2) scenario owing to the increase in modelled RO_2.

The HO_2 median measured to modelled (Missing k(OH) (OH to C96O2)) ratio vs NO in the middle panel increases from the measured to modelled (base) ratio at NO mixing ratios <1 ppbv, indicating improved agreement. At higher NO mixing ratios, where the base model begins to underpredict HO2, due to the large under-prediction in RO_2, this under-prediction is reduced in the missing k(OH) (OH to C96O2) scenario owing to the increase in modelled RO_2.

The OH median measured to modelled (Missing k(OH) (OH to C96O2)) ratio vs NO (top panel) highlights a missing OH source, the magnitude of which deceases as NO concentrations increase.

3. The experimental configuration of RO2 convertor is missing.

We have provided an experimental description of the RO_xLIF instrument on pg 6 and provide references to previous papers (Whalley et al., 2018 and Slater et al., 2020) where further details can be found. We will add details on the physical dimensions of the RO_2 convertor to the revised manuscript.

Pg6, line 176: In the RO_xLIF reactor, which is an 83 cm long, 6.4 cm internal diameter flow-tube, in HO_x-mode, a flow of CO (10% in N_2) was added just beneath the sampling inlet and this rapidly converted any ambient OH sampled to HO_2. Within the RO_xLIF FAGE cell, a continuous flow of NO (99.95%) titrated ambient HO_2, the converted OH and also a large % of RO_2-complex radicals (see below) to OH for detection. In RO_x-mode, a total-RO_2 + HO_2 + OH measurement was made by addition of a dilute flow of NO (500 ppmv in N_2) alongside the CO which promoted the conversion of all HO_2 and RO_2 radicals to OH; the OH formed was rapidly re-converted to HO2 by reaction with CO. Within the RO_xLIF FAGE cell, the HO_2 was titrated back to OH, by reaction with NO, for detection.

4. In Line 573, the estimated NO concentration is the reactor is 4e13 cm-3. The reaction time scale of RO2+NO reaction is 0.003s. If such large flow was used in the reactor, the conversion to OH could be finished and the OH could further react with NO to form HONO. How do the author account for such conversion?

Excess CO (CO:NO = 50) was added continuously to the ROxLIF reactor, so the dominant reaction of OH, once formed, was with CO to reform HO_2 rather than reaction with NO.

5. The RO2 and ROx budget is missing the part of Cl oxidation.

Nitryl chloride measurements were only made for part of the campaign period, so it is not possible to add the production of RO_2 radicals from Cl atoms to the campaign averages. We will add the following sentence to the revised manuscript to help the reader gauge the impact Cl oxidation rates can have on RO_2 production:

Pg16, line 488: The production rate of RO_2 from Cl-initiated VOC oxidation on these mornings would serve to enhance P(RO_x) by up to 2.1 ppbv hr^{-1}.

6. How sensitive of the experimental budget of HO2 and ROx radical towards the organic nitrate yield in the reaction of RO2 and NO? The organic nitrate yield varies from 0.01 to 0.5 among different RO2 species and it might have notable influence on the ROx and HO2 budget. Tan et al. (2019) not only set the yield to 0.05 but also performed the sensitivity tests by varying the yield from 5% to 20%, and notable influence was observed for their study although the bias was still within the experimental errors. Considering the large measured RO2 concentration, the yields might play significant role on this budget analysis in this study.

Increasing the alkyl nitrate yield will decrease the production rate of HO_2, and would lead to an improved agreement with the HO_2 destruction rate. However, an increased alkyl nitrate yield would serve to increase both the RO_2 and the total RO_x destruction rates, enhancing the discrepancy between the known RO_2 and RO_x production rates further. The MCM, which takes into account the different types of RO_2 present from the VOCs observed, predicts a mean alkyl nitrate yield of 6%, so we feel that our choice of a 5% yield in the budget analysis is appropriate.

7. If it was the case as the author said, 90% of the measured RO2 would react with NO to produce another RO2, in which the majority of the RO2 was probably derived from long-chain alkanes, monoterpenes, and other like-VOCs, this part of RO2 should be detected in the RO2-complex. According to Fig 5, the RO2-complex only made up less than 50% of the total RO2.

As we state on Pg 18, lines 566 – 569: both the simple- and complex-RO_2 species are enhanced (by including an alkoxy isomerisation mechanism in the model), as the first 3 generations of RO_2 species formed would be detected during the RO_x-mode in the RO_x-LIF instrument and, hence, contribute to RO_2-simple. The final RO_2 species formed, that does propagate to HO_2 via RO upon reaction with NO, would be detected during the HO_x-mode in the RO_xLIF instrument and, as such, contributes to the RO_2-complex fraction.

Besides, if the multiple bimolecular reaction of RO2 with NO made up such a proportion (90%), the ozone production would be inconceivably enhanced, but was not embodied in the observed O3 concentrations.

It is unwise to compare the ozone production rate to the observed ozone which will be impacted by physical processes such as advection, ventilation and deposition. The comparison of the model predicted glyoxal revealed that during the morning hours rapid ventilation effectively removed glyoxal from the model box. We can expect that ozone would be removed at the same rate and so the high rate of ozone production calculated from the observed peroxy radicals may not be reflected in the ozone concentration observed. We will comment on the losses of O_x in the revised manuscript. See response to Ezra Wood's comment.

Pg20, line 613 onwards: By approximating the rate of ozone production to the rate of NO_2 production from the reaction of NO with HO_2 and RO_2 radicals, urban radical measurements can be used to estimate chemical ozone formation (Kanaya et al., 2007; Ren et al., 2013; Brune et al., 2016; Tan et al., 2017; Whalley et al., 2018).

$$P(\mathrm{O_x}) = \left(k_{\mathrm{HO_2+NO}}[\mathrm{HO_2}][\mathrm{NO}] + k_{\mathrm{RO_2+NO}}[\mathrm{RO_2}][\mathrm{NO}]\right) \quad (11)$$

Losses of O_x ($L(O_x)$) include chemical losses such as the reaction of NO_2 with OH, net PAN formation, the fraction of $O(^1D)$ (formed by the photolysis of O_3) that react with H_2O and the reaction of O_3 with OH and HO_2. Physical

loss processes, such as O_3 deposition and ventilation out of the model box (see section 2.4) will also contribute to L(O_x). Physical processes such as advection of O_3 into the model box would also need to be considered in the model to make a direct comparison to the observed O_3 concentrations.

Considering the chemical production of O_x (E.11), recent studies where OH, HO_2 and RO_2 observations (via RO_xLIF) were made, demonstrated that models may under-predict ozone production at high NO due to an underestimation of the RO_2 radical concentrations at high NO concentrations (Tan et al., 2017; Whalley et al., 2018).

8. Line 563, Line 574-575, and Table 3, the author attributed the missing OH reactivity to additional reaction converting OH to C96O2, which is an α-pinene derived RO2, but C96O2 is formed in the α-pinene reaction with O3 but NOT with OH. How do the authors justify this assumption? Some discussion to make such assumption is needed.

This is true, our motivation for choosing C96O2 was to investigate the impact of RO isomerisation forming RO2 in the model and so picked the C96O2 peroxy radical as this species undergoes several isomerisation steps following RO_2+NO reaction and is already included in the MCM. We will add the following footnote to Table 3 in the revised manuscript to clarify this:

[1] Note, C96O2 is an α-pinene derived RO_2 that forms during the ozone-initiated oxidation of α-pinene. The additional production of C96O2 peroxy radicals in this model scenario was used to investigate the impact of an RO isomerisation mechanism on the modelled radical concentrations.

Technical comments:

1. Line 234, the last [RO2] should be out of the right bracket in Eq (6).

This will be corrected

2. Line 360, 'production and destruction'.

This will be corrected

3. There is no need for 2.4.1.

This will be removed and incorporated into section 2.4

4. Line 513, α = 0.87 seems to be wrong or the description of α was confusing.

The definition for alpha on page 17 line 513 should be α = 1 minus the rate at which RO forms RO2 or RC(O)O2 divided by the rate of RO conversion to HO2.

5. Conclusion should be section 4.

This will be corrected

Referee 2

This paper presents measurements of OH, HO2, and RO2 radical concentrations in addition to measurements of total OH reactivity in Beijing during the AIRPRO campaign in summer 2017. A radical budget analysis using the measured sources and sinks of these radicals revealed a potential missing source of OH during most of the campaign, although rates of OH production and destruction were in better balance under the higher NOx periods. The measured rates of HO2 production were found to be significantly greater than the rates of destruction, while the measured rates of destruction of RO2 radicals was found to be greater than the rates of production, especially under the higher NOx periods. These results suggest that the rate of conversion of RO2 to HO2 may be significantly slower than currently assumed. The authors also present the results of several 0-D box models using the MCM 3.3.1 chemical mechanism. The model was able to reproduce the measured OH concentrations, but underestimated the measured total OH reactivity, suggesting that the agreement may be fortuitous. The model also overestimated the measured HO2 concentrations and underestimated the measured RO2 concentrations, consistent with the experimental radical budget suggesting that the model may be overestimating the rate of conversion of RO2 to HO2 under high NO conditions. The model was found to be in better agreement with the measurements if the missing reactivity was assumed to be composed of VOCs that produced a-pinene derived RO2 radicals that upon reaction with NO results in isomerization reactions that reform other RO2 species before eventually producing HO2 effectively reducing the rate of conversion of RO2 radicals to HO2. While this model scenario improved the model agreement with the measurements of HO2 and RO2, it significantly underestimates the measured OH concentrations, consistent with a missing OH source. However, the proposed RO2 isomerization reactions may lead to the production of OH radicals and contribute to the missing OH source. The significant underestimation of the observed RO2 concentrations implies that the model is significantly underestimating the observed rate of ozone production under high NOx conditions. The measurements appear to be of high quality and include measurements of unknown interferences, which except for a few instances were found to be negligible. The measured radical concentrations are consistent with previous ROx measurements in several urban areas and is of interest to the atmospheric chemistry community. I recommend publication after the authors have addressed the following comments.

We thank referee 2 for their useful comments and have responded to each specific comment in bold below. The changes to the manuscript that we will make are in red.

1) The analysis generally focuses on the campaign average and the measurements under higher NOx conditions, but there is little discussion regarding the measurements under lower NO conditions, and in particular the extended period at the end of the campaign where the measured RO2 concentrations were the highest. The scale used in Figure 2 makes it difficult to see, but the discrepancy between the measurements and the model appears to be as significant as the discrepancies at higher NOx for this period. Unfortunately, this is not apparent from the information provided in Figure 6. It is not clear whether the additional VOC reactivity producing RO2 radicals that isomerize after reaction with NO to form additional RO2 would improve the model agreement for this period, as it is not clear whether reaction with NO still dominates the fate of peroxy radicals during this portion of the campaign. While the manuscript is already long, it would still benefit from a discussion of this aspect of their measurements.

We will extend the discussion on the model measurement comparison under the low NOx periods by including the following discussion:

Pg 14, line 440 onwards: The model under-estimates total RO$_2$ throughout the measurement period, although the level of disagreement (in terms of absolute concentration) is most severe from the 16th – 22nd June when NO concentrations were at their lowest. During this period, the average NO mixing ratio was ~0.4 ppbv during the afternoon hours, whilst the average NO mixing ratio for the entirety of the campaign was ~0.75 ppbv during the afternoons (Fig S1 in SI). The average peak NO mixing ratio observed in the morning (16th – 22nd June) was just over 6 ppbv, whilst the average peak NO mixing ratio for the entirety of the campaign was close to 16 ppbv.

Pg 18, line 566 onwards: The modelled radical concentrations predicted from the 'Missing k(OH) (OH to C96O2)' scenario are overlaid with the radical observations and modelled radicals from the base model scenario in Fig S2, SI. The additional VOC reactivity which produces RO$_2$ radicals that isomerise after reaction with NO is able to increase the modelled total RO$_2$ concentration both under the lower NO conditions experienced between the 16th – 22nd June as well as on the higher NO days 9th – 12th June indicating that NO is still at sufficient concentrations to dominate the fate of RO$_2$ between the 16th – 22nd June, despite NO concentrations being lower. The median measured to modelled (Missing k(OH) (OH to C96O2)) ratio vs NO (Fig S3, SI) highlights that the inclusion of alkoxy isomerisation following RO$_2$ + NO reaction increases the modelled RO$_2$ across the entire NO range but, considering the log scale, has the biggest impact on the ratio (from the measured to modelled (base) ratio) at the highest NO concentration. Both the simple- and complex-RO$_2$ species are enhanced, as the first 3 generations of RO$_2$ species formed would be detected during the RO$_x$-mode in the RO$_x$-LIF instrument and, hence, contribute to RO$_2$-simple.

Supplementary Information

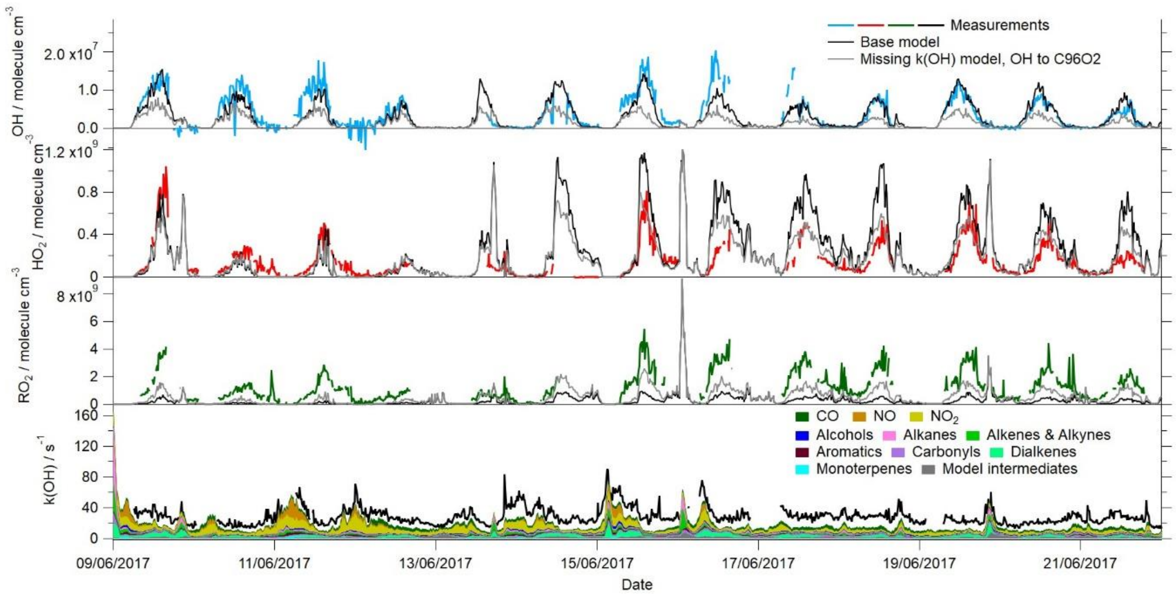

Figure S2: Time-series of the measured and modelled OH, HO_2, total RO_2 and OH reactivity from the 9th – 22nd June which encompasses high NO days (9th – 12th June) and low NO days (16th – 22nd June).

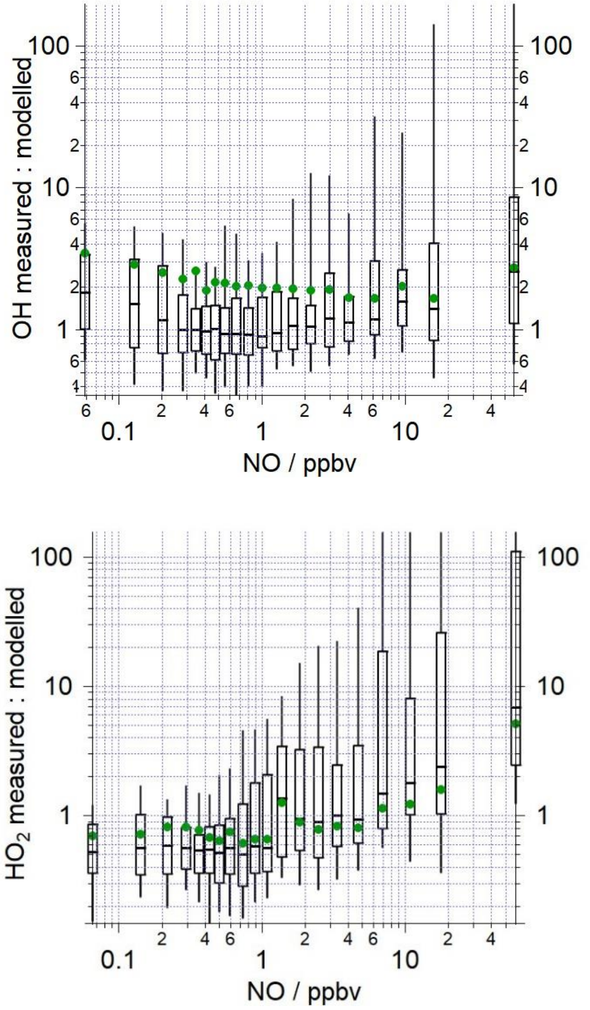

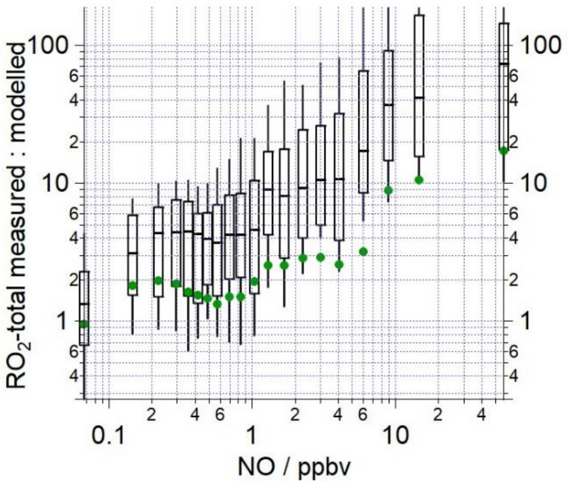

Figure S3: The median ratio (-) of the measured to modelled (base) OH, HO$_2$ and total RO$_2$ binned over the NO mixing ratio range encountered during the campaign on a logarithmic scale. The box and whiskers represent the 25th/75th and 5th/95th confidence intervals. The green circles display the measured to modelled OH, HO$_2$ and total RO$_2$ ratio when the model includes missing OH reactivity in the form of a single reaction which converts OH to C96O2. The number of data points in each of the NO bins is ~80

The median measured to modelled (Missing k(OH) (OH to C96O2)) ratio vs NO (green circles) is displayed in figure S3 alongside median measured to modelled (base) ratio. The inclusion of alkoxy isomerisation following RO$_2$ + NO reaction increases the modelled RO$_2$ concentration across the entire NO range but, considering the log scale, has the biggest impact on the ratio (from the measured to modelled (base) ratio) at the highest NO concentration. The HO$_2$ median measured to modelled (Missing k(OH) (OH to C96O2)) ratio vs NO in the middle panel increases from the measured to modelled (base) ratio at NO mixing ratios <1 ppbv, indicating improved agreement. At higher NO mixing ratios, where the base model begins to underpredict HO$_2$, due to the large under-prediction in RO$_2$, this under-prediction is reduced in the missing k(OH) (OH to C96O2) scenario owing to the increase in modelled RO$_2$.

The HO$_2$ median measured to modelled (Missing k(OH) (OH to C96O2)) ratio vs NO in the middle panel increases from the measured to modelled (base) ratio at NO mixing ratios <1 ppbv, indicating improved agreement. At higher NO mixing ratios, where the base model begins to underpredict HO2, due to the large under-prediction in RO$_2$, this under-prediction is reduced in the missing k(OH) (OH to C96O2) scenario owing to the increase in modelled RO$_2$.

The OH median measured to modelled (Missing k(OH) (OH to C96O2)) ratio vs NO (top panel) highlights a missing OH source, the magnitude of which deceases as NO concentrations increase.

2) Related to this, Berndt et al. (2018) report that RO2 + RO2 accretion reactions for a-pinene may be significant under low NOx conditions, and this type of accretion reaction may also be important for the peroxy radicals of other large VOCs. It's not clear whether these reactions could impact the modeled RO2 concentrations overall, but could be important during the low NOx period at the end of the campaign when the RO2 concentrations are high. Given that the authors are hypothesizing that isomerization of peroxy radicals of large VOCs produce additional peroxy radicals, the authors should comment on the potential impact of these reactions on the model results.

We have taken the rate of accretion from Berndt et al and the observed RO_2 and NO concentrations to assess if accretion reactions may be competitive under low NO conditions experienced. If we assume that all RO_2 species measured undergo accretion reactions with a rate coefficient of 9.7×10^{-12} cm^3 $molecule^{-1}$ s^{-1}, and compare this to the production rate of RO radicals from the reaction of RO_2 with NO we find that under the low NO_x period, the production rate of accretion products is comparable to the production rate of alkoxy radicals. If we use the faster rate coefficient of accretion of 79×10^{-12} cm^3 $molecule^{-1}$ s^{-1}, the production rate of accretion products is ~8.5 times faster than the RO production rate during the low NO_x period, although this should be viewed as an upper limit as the total RO_2 concentration measured will contain a contribution from small RO_2 radicals, such as CH_3O_2, for which the rate of accretion is negligible. Nevertheless, we expect the inclusion of accretion reactions in the MCM would serve to reduce the modelled RO_2 concentration under low NO_x conditions as the reaction represents a RO_x sink. This suggests that the missing RO_2 source may be even larger than reported here. Accretion reactions effectively remove RO_2 radicals without conversion of NO to NO_2 and so have implications for modelling in situ O_3 production, if models rely only on the rate of VOC oxidation when investigating O_3 production.

We will add the following discussion to the manuscript:

Pg 19, line 602 onwards: In addition to missing unimolecular RO_2 reactions, the model may be missing other RO_2 reaction pathways, for example, RO_2 accretion reactions, as identified by Berndt et al (2018). Although it is difficult to fully assess how competitive these RO_2+RO_2 reactions may be compared to RO_2+NO reactions from the total RO_2 observations made (the concentration of each individual RO_2 would be needed), the inclusion of accretion reactions in the MCM would serve to reduce the modelled RO_2 concentration under low NO_x conditions as the reaction represents an overall RO_x sink. This suggests that the missing RO_2 source identified may be even larger under the lower NO conditions.

Pg 20, line 609 onwards: Under low NO conditions there is emerging evidence that unimolecular isomerisation reactions occur for a range of RO_2 radicals (Jokinen et al., 2014; Ehn et al., 2014; Berndt et al., 2016; Wang et al., 2017b) as well as RO_2 accretion reactions (Berndt et al., 2018). These reactions will effectively remove RO_2 radicals without conversion of NO to NO_2 and so also have implications for modelling in situ O_3 production, if models rely only on the rate of VOC oxidation when investigating O_3 production.

3) The authors should provide plots of some of the diurnal averaged constraints for their model (NO, NO2, O3, CO, isoprene, etc.) to allow comparisons with other urban measurements and to put the results shown in Figure

5 into context. Adding the diurnal average of the low NOx period at the end of the campaign would also assist in interpreting the radical measurements during this period. This information could go into a supplement.

We will include the following figure in the SI to assist in the interpretation of the radical observations and for comparison with other urban measurements.

Supplementary Information

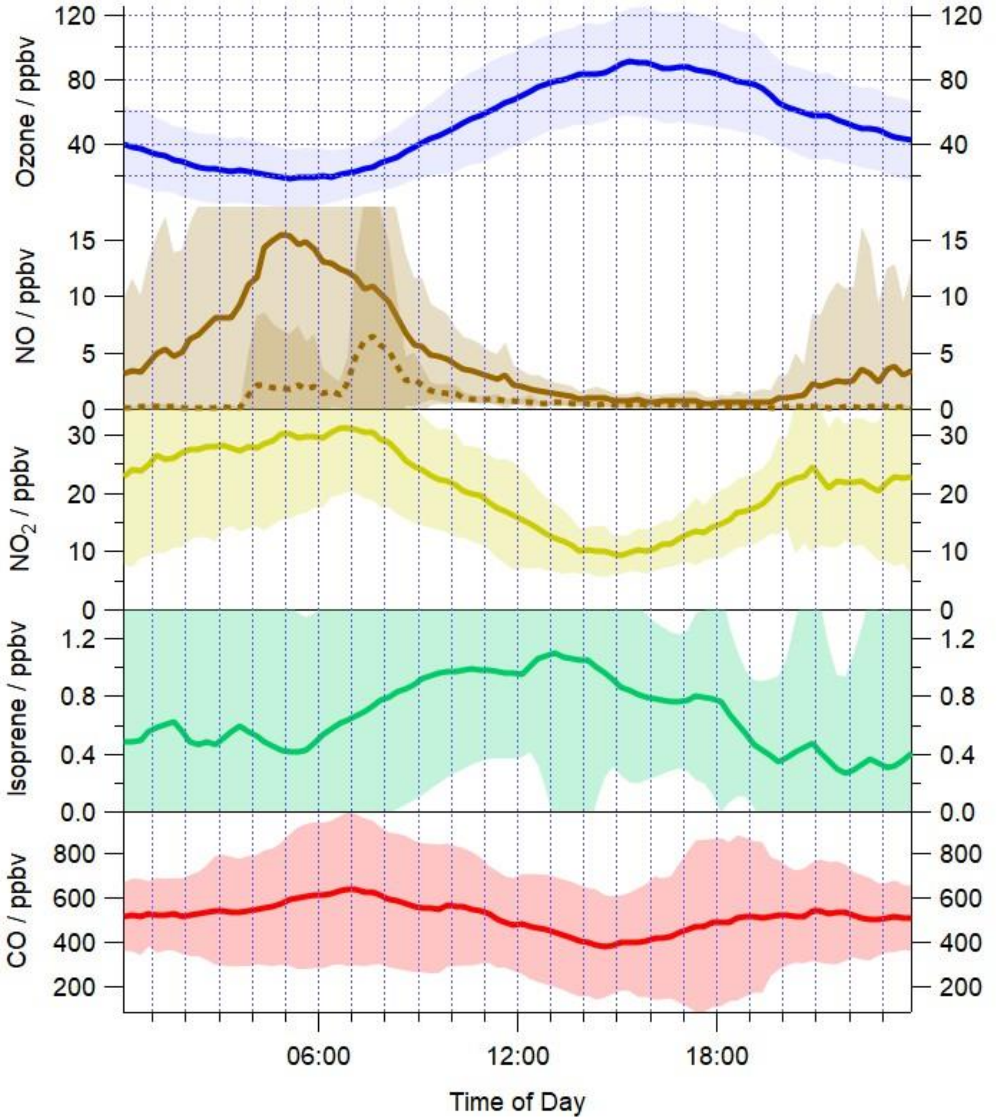

Figure S1: Average profiles for the observed O_3, NO, NO_2, isoprene, and CO at 15 minute intervals over 24 hours. The solid lines represent the campaign average whilst the dashed line is the average NO profile between 16th – 22nd June.

4) The definition of alpha on page 17 line 513 appears to be an error as it is not consistent with the value and the definition described on page 8 line 246. This should be clarified.

The definition for alpha on page 17 line 513 should be α = 1 minus the rate at which RO forms RO_2 or $RC(O)O_2$ divided by the rate of RO conversion to HO_2.

This will be changed in the revised manuscript.

Short comment by Ezra Wood

This paper presents some very interesting data and analysis from a study in Beijing using state of-the-art measurements of OH, HO2, and RO2. Similar to a few other recent studies, the authors find that RO2 concentrations and instantaneous ozone formation rates are both underestimated by 0-D models under high NOx conditions. The authors define the instantaneous rate of ozone production using Equation 11:

P(O3) = (kHO2+NO[HO2][NO] + kRO2+NO[RO2][NO]) −
(kOH+NO2+M[OH][NO2][M]+kRO2+NO2+M[RO2][NO2][M])

Similar definitions of P(O3) were used in Shirley et al. (2006), Sheehy et al. (2010), Dusanter et al. (2009), and Whalley et al. (2018), in contrast to the simpler earlier definitions which only included the first two terms on the right hand side of the equation, e.g., Kleinman et al. (1994), Thornton et al (2002), and Ren et al. (2003). The last two terms are included to account for the fact that O3 is not actually formed if an NO2 molecule formed by the reaction of NO with HO2 or RO2 is then immediately removed by reaction with OH to form HNO3 or with RO2 to form a peroxy nitrate. The problem with this definition is that those two NO2 removal reactions are just two of several Ox loss reactions, where [Ox] = [O] + [O3] + [NO2] + [O(1D)] + 2[NO3] + 3[N2O5]. For example, the reaction of O(1D) with H2O is just as much of an Ox loss mechanism as is the reaction of NO2 with OH. Including only one Ox loss term in the definition of P(O3) is confusing and not quite accurate. It would be much simpler and more accurate to just define the rate of gross Ox production as P(OX) = kHO2+NO[HO2][NO] + kRO2+NO[RO2][NO] and to separately define L(Ox), which would include the rates of the reactions OH + NO2, O(1D) + H2O, O3 + HO2, etc. The net rate of peroxy nitrate (RO2NO2) formation or loss could also be included. It is worth noting that truly defining the instantaneous formation rate of ozone (rather than Ox) necessitates accounting for variations in jNO2, e.g. P(O3) = jNO2[NO2] − k[NO][O3]. The difficulty of evaluating this expression and its limited utility, especially on days with variable jNO2 (due to clouds), underscore the advantage of considering Ox rather than O3.

Please note the similar open comments made for Dusanter et al., (2009): https://acp.copernicus.org/preprints/8/S5350/2008/acpd-8-S5350-2008.pdf References Dusanter, S., Vimal, D., Stevens, P. S., Volkamer, R., and Molina, L. T.: Measurements of OH and HO2 concentrations during the MCMA-2006 field campaign Part 1: Deployment of the Indiana University laser-induced fluorescence instrument, Atmos. Chem. Phys., 9, 1665-1685, 2009.**We thank Dr. Wood for his useful comment and agree that it would be more accurate to compare the modelled and measured P(O3) rather than the incomplete the net P(O3) that is in the manuscript currently. The loss terms in the calculation represent only a small subtraction and do not significantly change the differences reported between net P(O3) calculated from the measured and modelled peroxy radical concentrations. We will replace Figure 11 with the following figure which shows the modelled and measured P(O3) against NO and make the following changes to the text:**

Pg20, line 613 onwards: By approximating the rate of ozone production to the rate of NO_2 production from the reaction of NO with HO_2 and RO_2 radicals, urban radical measurements can be used to estimate chemical ozone formation (Kanaya et al., 2007; Ren et al., 2013; Brune et al., 2016; Tan et al., 2017; Whalley et al., 2018).

$$P(\mathrm{O_x}) = \left(k_{\mathrm{HO_2+NO}}[\mathrm{HO_2}][\mathrm{NO}] + k_{\mathrm{RO_2+NO}}[\mathrm{RO_2}][\mathrm{NO}]\right) \qquad (11)$$

Losses of O_x ($L(O_x)$) include chemical losses such as the reaction of NO_2 with OH, net PAN formation, the fraction of $O(^1D)$ (formed by the photolysis of O_3) that react with H_2O and the reaction of O_3 with OH and HO_2. Physical loss processes, such as O_3 deposition and ventilation out of the model box (see section 2.4) will also contribute to $L(O_x)$. Physical processes such as advection of O_3 into the model box would also need to be considered in the model to make a direct comparison to the observed O_3 concentrations.

Considering the chemical production of O_x (Eq.11), recent studies where OH, HO_2 and RO_2 observations (via RO_xLIF) were made, demonstrated that models may under-predict ozone production at high NO due to anunderestimation of the RO_2 radical concentrations at high NO concentrations (Tan et al., 2017; Whalley et al., 2018).

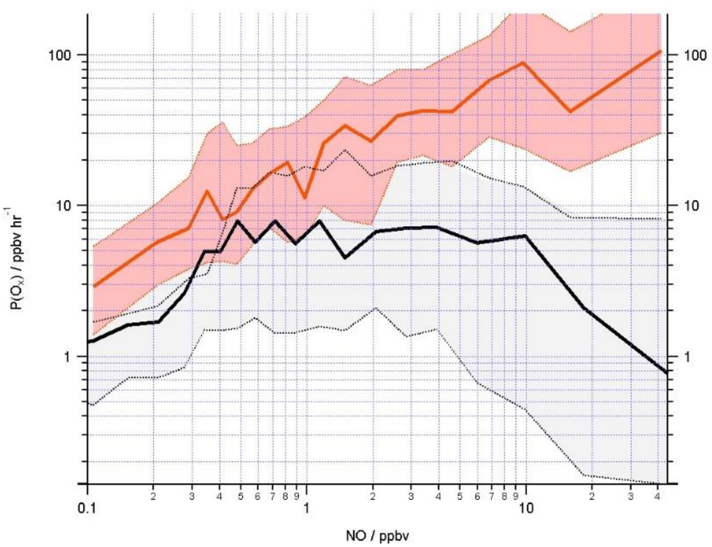

Figure 11: Mean O_x production (ppbv hr−1) calculated from observed (red line) and modelled (black line) RO_x concentrations using Eq. (11) binned over the NO mixing ratio range encountered during the campaign on a logarithmic scale. The shading represents the 25th / 75th percentile confidence limits. The number of data points in each of the NO bins is ~80

Evaluating the sensitivity of radical chemistry and ozone formation to ambient VOCs and NO_x in Beijing

Lisa K. Whalley[1,2], Eloise J. Slater[1], Robert Woodward-Massey[1,a], Chunxiang Ye[1,a], James D Lee[3,4], Freya Squires[4], James R. Hopkins[3,4], Rachel E Dunmore[4], Marvin Shaw[3,4], Jacqueline F. Hamilton[4], Alastair C Lewis[3,4], Archit Mehra[5,b], Stephen D. Worrall[5,c], Asan Bacak[5,d], Thomas J. Bannan[5], Hugh Coe[5,6], Carl J. Percival[7] Bin Ouyang[8~~7~~,e], Roderic L. Jones[8~~7~~], Leigh R. Crilley[9~~8~~,f], Louisa J. Kramer[9~~8~~], William J. Bloss[9~~8~~], Tuan Vu[9~~8~~], Simone Kotthaus[10~~9~~],[11~~0~~] Sue Grimmond[10~~9~~] Yele Sun[12~~1~~], Weiqi Xu[12~~1~~], Siyao Yue[12~~1~~], Lujie Ren[1~~1~~2], W. Joe F. Acton[1~~2~~3], C. Nicholas Hewitt[1~~2~~3], Xinming Wang[1~~3~~4], Pingqing Fu[1~~4~~5] and Dwayne E. Heard[1]

[1]School of Chemistry, University of Leeds, Leeds, LS2 9JT, UK
[2]National Centre for Atmospheric Science, University of Leeds, Leeds, LS2 9JT, UK
[3]National Centre for Atmospheric Science, University of York, Heslington, York, YO10 5DD, UK
[4]Wolfson Atmospheric Chemistry Laboratories, Department of Chemistry, University of York, Heslington, York, 10 YO10 5DD, UK
[5]Centre for Atmospheric Science, School of Earth and Environmental Sciences, The University of Manchester, Manchester, M13 9PL, UK
[6]National Centre for Atmospheric Science, University of Manchester, Manchester, M13 9PL, UK
[7]Jet Propulsion Laboratory, California Institute of Technology, USA
[8~~7~~]Department of Chemistry, University of Cambridge, UK
[9~~8~~]School of Geography, Earth and Environmental Sciences, University of Birmingham, B15 2TT, Birmingham, UK
[10~~9~~] Department of Meteorology, University of Reading, Reading, UK
[11~~0~~]Institut Pierre Simon Laplace, École Polytechnique, Palaiseau, France
[12~~1~~]State Key Laboratory of Atmospheric Boundary Layer Physics and Atmospheric Chemistry, Institute for Atmospheric Physics, Chinese Academy of Sciences, 40 Huayanli, Chaoyang District, Beijing 100029, China
[1~~2~~3]Lancaster Environment Centre, Lancaster University, Lancaster, LA1 4YW, UK
[1~~3~~4]State Key Laboratory of Organic Geochemistry, Guangzhou Institute of Geochemistry, Chinese Academy of Sciences, 511 Kehua Street, Wushan, Tianhe District, Guangzhou, GD 510640 , China
[15~~3~~]Institute of Surface-Earth System Science, Tianjin University, Tianjin 300072, China
[a]Now at: College of Environmental Sciences and Engineering, Peking University, Beijing, 100871, China
[b]Now at: Faculty of Science and Engineering, University of Chester, CH2 4NU, UK
[c]Now at: Aston Institute of Materials Research, School of Engineering and Applied Science, Aston University, Birmingham, B4 7ET, UK
[d]Now at: Turkish Accelerator & Radiation Laboratory, Ankara University Institute of Accelerator Technologies, Atmospheric and Environmemtal Chemistry Laboratory, Gölbaşı Campus, Ankara, Turkey
[e]Now at: Lancaster Environment Centre, Lancaster University, Lancaster, LA1 4YW, UK

[f]Now at: Department of Chemistry, York University, Toronto ON, M3J 1P3, Canada

Correspondence to: Lisa Whalley (l.k.whalley@leeds.ac.uk)

Abstract. Measurements of OH, HO_2, RO_2-complex (alkene and aromatic-related RO_2) and total RO_2 radicals taken during the AIRPRO campaign in central Beijing in the summer of 2017, alongside observations of OH reactivity are presented. The concentrations of radicals were elevated with OH reaching up to 2.8 x 10^7 molecule cm^{-3}, HO_2 peaked at 1 x 10^9 molecule cm^{-3} and the total RO_2 concentration reached 5.5 x 10^9 molecule cm^{-3}. OH reactivity (k(OH)) peaked at 89 s^{-1} during the night, with a minimum during the afternoons of ~22 s^{-1} on average. An experimental budget analysis, in which the rates of production and destruction of the radicals are compared, highlighted that although the sources and sinks of OH were balanced under high NO concentrations, the OH sinks exceeded the known sources (by 15 ppbv hr^{-1}) under the very low NO conditions (<0.5 ppbv) experienced in the afternoons, demonstrating a missing OH source consistent with previous studies under high volatile organic compound (VOC), low NO loadings. Under the highest NO mixing ratios (104 ppbv), the HO_2 production rate exceeded the rate of destruction by ~ 50 ppbv hr^{-1}, whilst the rate of destruction of total-RO_2 exceeded the production by the same rate indicating that the net propagation rate of RO_2 to HO_2 may be substantially slower than assumed. If just 10% of the RO_2 radicals propagate to HO_2 upon reaction with NO, the HO_2 and RO_2 budgets could be closed at high NO, but at low NO this lower RO_2 to HO_2 propagation rate revealed a missing RO_2 sink that was similar in magnitude to the missing OH source. A detailed box model that incorporated the latest MCM chemical mechanism (MCM3.3.1) reproduced the observed OH concentrations well, but over-predicted the observed HO_2 under low concentrations of NO (<1 ppbv) and under-predicted RO_2 (both the complex-RO_2 fraction and other RO_2 types which we classify as simple-RO_2) most significantly at the highest NO concentrations. The model also under-predicted the observed k(OH) consistently by ~10 s^{-1} across all NO_x levels highlighting that the good agreement for OH was fortuitous due to a cancellation of missing OH source and sink terms in its budget. Including heterogeneous loss of HO_2 to aerosol surfaces did reduce the modelled HO_2 concentrations in-line with the observations, but only at NO mixing ratios <0.3 ppbv. The inclusion of Cl atoms, formed from the photolysis of nitryl chloride, enhanced the modelled RO_2 concentration on several mornings when the Cl atom concentration was calculated to exceed 1 x 10^4 atoms cm^{-3} and could reconcile the modelled and measured RO_2 concentrations at these times. However, on other mornings, when the Cl atom concentration was lower, large under-predictions in total RO_2 remained. Furthermore, the inclusion of Cl atom chemistry did not enhance the modelled RO_2 beyond the first few hours after sunrise and so was unable to resolve the modelled under-prediction in RO_2 observed at other times of the day. Model scenarios, in which missing VOC reactivity was included as an additional reaction that converted OH to RO_2, highlighted that the modelled OH, HO_2 and RO_2 concentrations were sensitive to the choice of RO_2 product. The level of modelled to measured agreement for HO_2 and RO_2 (both complex and simple) could be improved if the missing OH reactivity formed a larger RO_2 species that was able to undergo reaction with NO, followed by isomerisation reactions reforming other RO_2 species, before eventually generating HO_2. In this work an α-pinene-derived RO_2 species was used as an example. In this simulation, consistent with the experimental budget analysis,

the model underestimated the observed OH indicating a missing OH source. The model uncertainty, with regards to the types of RO_2 species present and the radicals they form upon reaction with NO (HO_2 directly or another RO_2 species), leads to over an order of magnitude less O_3 production calculated from the predicted peroxy radicals than calculated from the observed peroxy radicals at the highest NO concentrations. This demonstrates the rate at which the larger RO_2 species propagate to HO_2 or to another RO_2 or indeed to OH needs to be understood to accurately simulate the rate of ozone production in environments such as Beijing where large multifunctional VOCs are likely present.

1 Introduction

Owing to strict emission controls being implemented across China, a reduction in the levels of PM_{10}, $PM_{2.5}$ and SO_2 have been observed in the country since 2013 (Huang et al., 2018). Similar reductions in these primary pollutants are echoed in other countries across the globe. In the US this reduction in primary emissions is reflected in a ~0.4 ppbv yr^{-1} reduction in peak O_3 (He et al., 2020). In China, however, despite reductions in primary emissions, the concentration of ground-level ozone has been gradually increasing between 2013 – 2017 (Huang et al., 2018). The highest peak ozone concentrations in China are observed in the Beijing area (Wang et al., 2017a) where the highest O_3 mixing ratio of 286 ppbv was recorded at a rural site 50 km north of the centre (Wang et al., 2006). During the Beijing Olympic Games, despite emission controls, hourly ozone mixing ratios between 160 to 180 ppbv were frequently observed in central Beijing (Wang et al., 2010). Ozone is a secondary pollutant, primarily formed in the troposphere via OH-initiated VOC oxidation in the presence of NO_x. O_3 concentrations in megacities worldwide frequently exceed regulatory limits during the summer months, with elevated ozone concentrations shown to have negative impacts on human and crop health. The radical species, OH, HO_2 and RO_2 play a central role in the catalytic photochemical cycle which removes primary emissions and leads to ozone formation. The OH radical initiates the oxidation of VOCs leading to the formation of peroxy radicals (HO_2 and RO_2). Peroxy radicals oxidise NO to NO_2 which photolyses and generates ozone. Under high NO_x conditions, OH preferentially reacts with NO_2, and both peroxy radical production (via VOC oxidation) and, in turn, ozone production decreases. This non-linear relationship between ozone and NO_x complicates efforts to reduce the ambient ozone levels as, in NO_x-saturated environments, reductions in NO_x can lead to increases in the rate of ozone production (e.g. (Bigi and Harrison, 2010)). Furthermore, a number of studies have highlighted that efforts to reduce PM have the potential to exacerbate O_3 due to concomitant increases in HO_2 caused by a reduction in the heterogeneous loss of HO_2 to aerosol surfaces (Li et al., 2019), although there is continued debate on the magnitude of this effect from field studies (Tan et al., 2020). As well as the central role OH plays in photochemical ozone formation, OH promotes the formation of secondary aerosols (sulphate, nitrate and secondary organic aerosols (SOA)) which have negative impacts on human health (Chen et al., 2013). Large, complex RO_2 radicals are precursors to highly oxidised molecules (HOMs) (Ehn et al., 2014) also which have been shown to condense and contribute to SOA (Mohr et al., 2019). In China, the fraction of PM attributed to secondary aerosols is significant (between 44 – 71%, (Huang et al., 2014)) and so understanding the oxidation chemistry which converts primary emissions to secondary aerosols is an ongoing challenge. There has been an increasing growth in photochemical oxidant studies conducted in China where radical observations have been performed over the past decade with the PKU and Juelich groups leading these efforts. The first radical observations took place in the summer of 2006 with observations made in the Pearl River Delta region (Hofzumahaus et al., 2009; Lu et al., 2012) (PRIDE-PRD-2006) and also in suburban Beijing (Lu et al., 2013) (CareBeijing2006). These campaigns revealed a strong atmospheric oxidation capacity with elevated levels of OH and HO_2 in these regions, with OH concentrations up to 2.6 x 10^7 molecule cm^{-3} and HO_2 concentrations up to 2.5 x 10^9 molecule cm^{-3} reported (Lu et al., 2012). Even during the wintertime, under low levels of solar radiation, concentrations of OH can reach 3 × 10^6 molecule cm^{-3} in Beijing (Slater et al., 2020) which is similar to the OH concentrations observed in other urban centres in European cities during the summer months (Whalley et al., 2018). Similar to findings from radical observations and subsequent modelling activities in forested regions (Whalley et al., 2011), which are characterised by high VOC emissions and relatively low NO_x concentrations, the observations and modelling studies in China in summer (Hofzumahaus et al., 2009; Lu et al., 2012; Lu et al., 2013) revealed that the high OH concentrations could only be explained if an additional source of OH, from recycling peroxy radicals to OH, was added to the model. An updated isoprene scheme (Peeters et al., 2009; Peeters et al., 2014) which included isomerisation reactions of the isoprene-derived RO_2 radicals, was unable to reconcile the OH observations, however. In a subsequent field study conducted in the PRD region (Tan et al., 2019), RO_2 observations were made using the RO_xLIF technique alongside OH, HO_2 and OH reactivity allowing an experimental budget analysis for OH, HO_2, RO_2 and RO_x (OH + HO_2 + RO_2) to be performed. The analysis demonstrated a missing OH source of 4 – 6 ppbv hr^{-1} and a missing RO_2 sink that was similar in magnitude and, hence, supports the hypothesis of a missing mechanism that converts RO_2 species to OH under low NO conditions. The authors calculated that the unknown RO_2 to OH conversion that does not involve reaction with NO (and, therefore, does not lead to the formation of ozone) reduced ozone production by 30 ppbv per day demonstrating that knowledge of the branching ratio between the competitive reactions that RO_2 radicals undergo (bimolecular reaction with NO or unimolecular isomerisation), as well as the overall VOC oxidation rate, is important when determining in situ ozone production.

In a recent campaign conducted at a rural site in the North China Plain (Tan et al., 2017), during periods for which NO mixing ratios were below 300 pptv, an additional OH recycling mechanism was again needed to reconcile the OH concentrations observed. The modelled RO_2 concentrations were in good agreement with those observed under low NO concentrations typically experienced during the afternoon, however, the model under-predicted the RO_2 concentrations by a factor of 3 - 5 at the higher NO mixing ratios (>1 ppbv) that were observed during the mornings. Additional sources of RO_2 from the photolysis of $ClNO_2$ and subsequent reactions of Cl atoms with VOCs, as well as RO_2 from the missing reactivity determined, could explain ~ 10 – 20% of the model under-prediction, but could not fully resolve the missing RO_2 source of 2ppbv hr^{-1} under the high NO conditions. As a result, the model was found to under-predict the net in situ chemical ozone production by 20 ppbv per day. In London, during the ClearfLo campaign (Whalley et al., 2018), under higher NO mixing ratios (> 3ppbv) a box model constrained to the MCM3.2 was found to increasingly under-predict the RO_2 concentrations observed with NO_x and, as a consequence the rate of ozone production calculated from the modelled peroxy radical concentrations was up to an order of magnitude lower than the ozone production rate calculated from the observed peroxy radicals. The model was able to reproduce the observed levels of HO_2 under the high NO concentrations, but over-predicted HO_2 concentrations when NO mixing ratios were below 1 ppbv and modest under-predictions of OH were observed under low NO conditions which demonstrated uncertainties in radical cycling at low NO. Conversely, in other urban studies, models were found to increasingly under-predict HO_2 as NO_x levels increased beyond ~ 1 ppbv (Martinez et al., 2003; Ren et al., 2013; Brune et al., 2016) although in some of these earlier studies, the HO_2 observations may have been influenced by an RO_2 interference (Whalley et al., 2013). Understanding the cause of the model failure under different NO regimes in urban centres is critical to be able to accurately predict ozone production and to determine ozone abatement strategies that can be implemented to successfully reduce ozone levels. Measurements of OH, HO_2 and RO_2 as well as OH reactivity are necessary to fully explore a model’s skill to capture the entire atmospheric oxidation cycle and to begin to identify mechanisms that can reconcile the concentration of all radical species.

The integrated Study of AIR Pollution PROcesses in Beijing (AIRPRO) project involved two intensive measurement periods that took place in central Beijing during the winter of 2016 and during the following summer of 2017 and was part of the larger Air Pollution and Human Health (APHH) program. APHH had the overall aim of better understanding the sources, atmospheric transformations and health impacts of air pollutants in Beijing to improve air quality forecasting capabilities (Shi et al., 2019). In this paper the observations of OH, HO_2, RO_2 and OH reactivity from the summer period are compared to a detailed zero dimensional box model run with the latest Master Chemical Mechanism (MCM3.3.1) and an experimental budget analysis is performed on all radical species. The overall objective of this research was to test the model’s ability to reproduce the radical concentrations and, through the budget analysis investigate the balance between radical production and destruction rates. Following on from the results of earlier radical observation and modelling studies conducted in urban regions, this research will investigate if there are missing radical sources and sinks under different NO regimes and investigate new chemistry that may improve model predictions. We will assess how uncertainties in the model mechanism influence the rate of in situ ozone production in an environment with large and complex VOC emissions and under highly variable NO_x concentrations.

2 Experimental

2.1 Site description

The observations took place in central Beijing at the Institute of Atmospheric Physics (IAP), which is part of the Chinese Academy of Sciences. The site was located between the third and fourth north ring roads in Beijing and was within 150 m of several busy roads. All instrumentation was located in close proximity within 9 shipping containers that were placed on a grassed area surrounding a large (325 m) meteorological tower. Further details of the measurement site and an overview of all the instrumentation that was run during the campaign can be found in Shi et al., (2019).

2.2 FAGE instrumentation

The University of Leeds fluorescence assay by gas expansion (FAGE) instrument was deployed at the IAP site and made measurements of OH, HO_2, RO_2 radicals and OH reactivity (k(OH)). The instrumental set-up was analogous to that used during the ClearfLo project (see Whalley et al., (2016) for the k(OH) instrument description and Whalley et al., (2018) for the OH, HO_2, and RO_2 instrument details) and also the winter AIRPRO project (Slater et al., 2020) and so is only briefly overviewed here. Two detection cells, the HO_x cell and the RO_xLIF cell, were located on the roof of the Leeds FAGE shipping container at a sampling height of 3.5 m. The k(OH) instrument, which was housed inside the container, alongside all other FAGE instrument components (including the laser system), drew air from close by the radical detection cells via an ½” Teflon line. The HO_x cell made sequential measurements of OH and then the sum of OH + HO_2, by the addition of NO (Messer, 99.95%) which titrated HO_2 to OH for detection by laser induced fluorescence (LIF). In the RO_xLIF reactor, which is an 83 cm long, 6.4 cm internal diameter flow-tube, in HO_x-mode, a flow of CO (10% in N_2) was added just beneath the sampling inlet and this rapidly converted any ambient OH sampled to HO_2. Within the RO_xLIF FAGE cell, a continuous flow of NO (99.95%) titrated ambient HO_2, the converted OH and also a large % of RO_2-complex radicals (see below) to OH for detection. In RO_x-mode, a total-RO_2 + HO_2 + OH measurement was made by addition of a dilute flow of NO (500 ppmv in N_2) alongside the CO which promoted the conversion of all HO_2 and RO_2 radicals to OH; the OH formed was rapidly re-converted to HO_2 by reaction with CO. Within the RO_xLIF FAGE cell, the HO_2 was titrated back to OH, by reaction with NO, for detection. Using the methodology outlined in Whalley et al., (2013) the sensitivity of both the HO_x and RO_xLIF FAGE cells towards HO_2 and RO_2-complex species was assessed before the instrument was deployed to Beijing by sampling isoprene-derived RO_2; the sensitivity of the HO_x cell towards other RO_2 types such as those derived from ethene, methanol and propane has been previously conducted (Whalley et al., 2013) and compared well with model-predicted sensitivities. The sensitivity of the ROxLIF instrument has also been assessed previously towards a range of RO_2 types deriving from methane, isoprene, ethene, toluene, butane and cyclohexane and, again, compared well with model-predicted sensitivities (Whalley et al., 2018). RO_2-complex refers to any RO_2 species (primarily those derived from alkene and aromatic hydrocarbons) that have the potential to decompose into OH in the presence of NO on the time-scale of the FAGE residence time and, therefore, have the potential to act as an HO_2 interference. The NO flow in the HO_x cell was kept low to minimise the conversion efficiency of RO_2-complex to OH and the conversion efficiency was found to be <5% when isoprene-derived RO_2 radicals were sampled. In the RO_xLIF FAGE cell, a higher NO flow was employed to promote the conversion of RO_2-complex to OH, enabling 89% of isoprene-derived RO_2 radicals to be detected. From the relative sensitivities of the two cells to OH, HO_2 and RO_2-complex, and by subtraction of RO_2-complex from total RO_2, the concentration of RO_2 species that do not act as an HO_2 interference (RO_2-simple) has been derived.

For the entirety of the campaign, the HO_x cell was equipped with an inlet-pre-injector (IPI) (Woodward-Massey et al., 2020) which, by injection of propane into the ambient air-stream directly above the HO_x inlet, removes ambient OH and enables a background measurement from laser scatter, solar scatter and detector dark counts (and potentially any cell-generated OH) to be determined whilst the laser is tuned to the OH transition. The subtraction of this background signal from the ambient OH signal provides the OH_{CHEM} measurement which can be compared to the traditional OH_{WAVE} measurement in which the background signal (from laser scatter, solar scatter and detector dark counts only) is determined by tuning the laser wavelength away from the OH transition. Differences between OH_{CHEM} and OH_{WAVE} can highlight the presence of an OH interference. During the summer AIRPRO campaign, once the known OH interference deriving from laser-photolysis of ambient ozone and the subsequent reaction of photogenerated $O(^1D)$ atoms with ambient H_2O (v) was accounted for (Woodward-Massey et al., 2020) the agreement between OH_{CHEM} and OH_{WAVE} was generally very good (see figure 14 in Woodward-Massey et al., (2020)). However, on five afternoons when ozone was extremely elevated (>100 ppbv) and OH concentrations were high ($>1\times10^7$ cm^{-3}), OH_{WAVE} was greater than OH_{CHEM} (by up to 18 %) highlighting a small unknown interference under these very perturbed conditions. In all the model-measurement comparisons presented in the section 3, the interference-free OH_{CHEM} measurement is used.

Both detection cells were calibrated every 3 days during the campaign by photolysis of a known concentration of H_2O (v) at 185 nm with a Hg lamp in synthetic air (Messer, Air Grade Zero 2) within a turbulent flow tube which generates an equal concentration of OH and HO_2 (Whalley et al. 2018). The product of the photon flux at 185 nm (determined by N_2O actinometry (Commane et al., 2010) before and after the instrument was deployed to Beijing), $[H_2O]$ and irradiance time, was used to calculate [OH] and $[HO_2]$. For calibration of RO_2 concentrations, methane (Messer, Grade 5, 99.99%) was added to the humidified air flow in sufficient quantity to completely convert OH to CH_3O_2. The median limit of detection (LOD) during the campaign was 6.1×10^5 molecule cm^{-3} for OH, 2.8×10^6 molecule cm^{-3} for HO_2 and 7.2×10^6 molecule cm^{-3} for CH_3O_2 at a typical laser power of 11 mW for a 5 minute data acquisition cycle (SNR=2). The field measurements of all species were recorded with 1 s time-resolution, and the precision of the measurements was calculated using the standard errors in both the online and offline points. The accuracy of the measurements was ~ 26 % (2σ), and is derived from untertainties in the calibration, which derives largely from that of the chemical actinometer (Commane et al., 2010).

2.3 Experimental budget analysis

An experimental budget analysis has been conducted for OH, HO_2, RO_2, and total RO_x following the approach outlined in Tan et al., (2019) and which relies only on field-measured quantities (concentrations and photolysis rates) and published chemical kinetic data, and not any model calculated concentrations. The rates of production and destruction of each radical species is calculated using equations 1 – 8 below.

$$P_{\mathrm{OH}} = j_{\mathrm{HONO}}[\mathrm{HONO}] + (2f \times j_{\mathrm{O^1D}}[\mathrm{O_3}]) + \sum i\{\varphi^{i}{}_{\mathrm{OH}} k^{i}{}_{1}[\mathrm{alkene}]_i[\mathrm{O_3}]\} + (k_2[\mathrm{NO}] + k_3[\mathrm{O_3}])[\mathrm{HO_2}] \qquad (1)$$

$$D_{\mathrm{OH}} = [\mathrm{OH}]k_{\mathrm{OH}} \qquad (2)$$

$$P_{\mathrm{HO_2}} = 2j_{\mathrm{HCHO\_r}}[\mathrm{HCHO}] + \sum i\left\{\varphi^{i}{}_{\mathrm{HO_2}} k^{i}{}_{1}[\mathrm{alkene}]_i[\mathrm{O_3}]\right\} + (k_4[\mathrm{HCHO}] + k_5[CO])[OH] + \alpha k_6[\mathrm{NO}][\mathrm{RO_2}] \qquad (3)$$

$$D_{\mathrm{HO_2}} = (k_7[\mathrm{NO}] + k_8[\mathrm{O_3}] + k_9[\mathrm{RO_2}] + k_{\mathrm{het}} + 2k_{10}[\mathrm{HO_2}])[\mathrm{HO_2}] \qquad (4)$$

$$P_{\mathrm{RO_2}} = \sum i\left\{\varphi^{i}{}_{\mathrm{RO_2}} k^{i}{}_{1}[\mathrm{alkene}]_i[\mathrm{O_3}]\right\} + k_{\mathrm{OH}}[\mathrm{VOC}][\mathrm{OH}] \qquad (5)$$

$$D_{\mathrm{RO_2}} = \{(\alpha + \beta)k_6[\mathrm{NO}] + (2k_{11}[\mathrm{RO_2}] + k_9[\mathrm{HO_2}])\cancel{[\mathrm{RO_2}]}\}[\mathrm{RO_2}] \qquad (6)$$

$$P_{\mathrm{RO_x}} = j_{\mathrm{HONO}}[\mathrm{HONO}] + 2f \times j_{\mathrm{O^1D}}[\mathrm{O_3}] + 2j_{\mathrm{HCHO\_r}}[\mathrm{HCHO}] + \sum i\left\{(\varphi^{i}{}_{\mathrm{OH}} + \varphi^{i}{}_{\mathrm{HO_2}} + \varphi^{i}{}_{\mathrm{RO_2}})k^{i}{}_{1}[\mathrm{alkene}]_i[\mathrm{O_3}]\right\} \qquad (7)$$

$$D_{\mathrm{RO_x}} = (k_{12}[\mathrm{NO_2}] + k_{13}[\mathrm{NO}])[\mathrm{OH}] + \beta k_6[\mathrm{NO}][\mathrm{RO_2}] + 2(k_{11}[\mathrm{RO_2}]^2 + k_9[\mathrm{RO_2}][\mathrm{HO_2}] + k_{10}[\mathrm{HO_2}]^2) \qquad (8)$$

where j_{HONO} and $j_{\mathrm{O^1D}}$ are the measured photolysis rates of HONO and O_3 (forming O^1D) respectively, f is the fraction of O^1D radicals that react with H_2O rather than are collisionally quenched to $O(^3P)$ ($f = 0.1$ on average) and $\varphi^{i}{}_{\mathrm{OH}}$, $\varphi^{i}{}_{\mathrm{HO_2}}$, $\varphi^{i}{}_{\mathrm{RO_2}}$ and $k^{i}{}_{1}$ are the yield of OH, HO_2 and RO_2 from, and rate coefficients for, individual ozone-alkene reactions taken from the MCM3.3.1 respectively. $j_{\mathrm{HCHO\_r}}$ is the measured HCHO photolysis rate that yields HO_2 radicals, k_{het} is the first order loss of HO_2 to the measured aerosol surface area, calculated using Eq.9:

$$k_{\mathrm{het}} = \frac{\omega A \gamma}{4} \qquad (9)$$

where ω is the mean molecular speed of HO_2 (equal to 43725 cm s^{-1} at 298 K), γ is the aerosol uptake coefficient (0.2 is used here as recommended by Jacob (2000)) and *A* is the measured aerosol surface area in cm^2cm^{-3}. α is the fraction of RO_2 radicals that upon reaction with NO propagate to HO_2 rather than reform another RO_2 radical; initially $\alpha = 1$ has been assumed. β is the fraction of RO_2 radicals that upon reaction with NO form alkyl nitrates and is set to 0.05 as used by Tan et al., (2019) to represent an average alkyl nitrate yield for the various types of RO_2 species likely present. All rate coefficients ($k_1 - k_{13}$) used are listed in Table 1 and the concentration of species used in the budget analysis are the concentrations that were observed during the campaign.

2.4 MCM3.3.1 box model description

A zero-dimensional (box) model incorporating the Master Chemical Mechanism (MCM3.3.1) (Jenkin et al., 2015) (http://mcm.leeds.ac.uk/MCM/home) was used to predict the radical concentrations and OH reactivity for comparison with the observations. The model was constrained by measurements of NO, NO_2, NO_3, O_3, CO, HCHO, HNO_3, HONO, water vapour, temperature, pressure and individual VOC species measured by DC-GC-FID (dual-channel gas chromatography with flame ionisation) and PTR-ToF-MS (proton transfer reactor-time of flight-mass spectrometry). Table 2 lists the different VOC species measured. HCHO was measured using a recently developed LIF instrument with 1 sec time resolution and LOD of 80 pptv (Cryer, 2016). HONO was measured by a long-path absorption photometer (LOPAP) and broadband cavity-enhanced absorption spectrophotometry (BBCEAS) and the HONO concentration as recommended in Crilley et al., (2019) are used here. Further details on all instrumentation deployed during the campaign is overviewed in Shi et al. (2019).

The model was constrained with the measured photolysis frequencies j(O^1D), j(NO_2) and j(HONO)), which were calculated from the measured wavelength-resolved actinic flux and published absorption cross sections and photodissociation quantum yields. For other species which photolyse at near-UV wavelengths (<360 nm), such as HCHO and CH_3CHO, the photolysis rates were calculated by scaling to the ratio of clear-sky j(O^1D) to observed j(O^1D) to account for clouds. For species which photolyse further into the visible the ratio of clear-sky j(NO_2) to observed j(NO_2) was used. The variation of the clear-sky photolysis rates (j) with solar zenith angle (χ) was calculated within the model using the following expression:

$$j = l\cos(\chi)m \times e - n\sec(\chi) \qquad (10)$$

with the parameters *l*, *m* and *n* optimised for each photolysis frequency (see Table 2 in Saunders et al., (2003)). The model inputs were updated every 15 minutes, the species that were measured more frequently were averaged to 15 minutes whilst the measurements with lower time resolution were interpolated. To estimate how long model generated intermediate species survive before being physically removed by processes such as deposition or ventilation, the model was left unconstrained to glyoxal and the rate of physical loss was varied. The model was able to reproduce the observed glyoxal concentrations if a deposition velocity of 0.5 cm s^{-1} was used, combined with a ventilation term that increased with boundary layer depth. As the boundary layer gradually increased in the morning, the lifetime of glyoxal with respect to ventilation was ~ 1 hour, whilst at night the lifetime gradually increased to ~ 5 hours; this variable lifetime was applied to all model-generated species. As a further check on the physical loss rate imposed, the model was run unconstrained to HCHO using the same deposition rates and was found to reproduce the observed HCHO concentrations that were observed during the daytime, but under-predicted the concentrations at night, potentially indicating that primary emissions of HCHO as well as secondary production contributed to the observed concentrations. In all the model scenarios presented in section 3, the observed HCHO concentration is used. The model was run for the entirety of the campaign in overlapping 7 day segments. To allow all the unmeasured, model generated intermediate species time to reach steady state concentrations, the model was initialised with inputs from the first measurement day and spun-up for 2 days before comparison to measurements of OH, HO_2, RO_2 and k(OH) were made. For comparison of the modelled RO_2 to the observed RO_2-total, RO_2-complex and RO_2-simple, the RO_xLIF instrument sensitivity towards each RO_2 species in the model was determined by running a model first under the RO_xLIF reactor and then the RO_xLIF FAGE cell conditions (NO concentrations and residence times) to determine the conversion efficiency of each modelled RO_2 species to HO_2.

~~2.4.1 Model descriptions~~

A series of model runs have been performed and are summarised in Table 3:

3 Results and Discussion

3.1 Overview of the chemistry and meteorology during the campaign

As part of the AIRPRO project, gas-phase, aerosol, and meteorological observations were made at the IAP site from the 21st May to 26th June in 2017. Typically clear skies and elevated temperatures prevailed, with rain on just a few days. Temperatures frequently exceeded 35 °C whilst $j(O^1D)$ peaked at just over 3×10^{-5} s^{-1} at noon (Figure 1). The dominant wind direction reaching the site during the summer was from the southwest and the measured hourly mean wind speed was 3.6 ms^{-1} (Shi et al., 2019). Despite the close proximity of the measurement site to the heavily trafficked Jingzang highway in Beijing, mixing ratios of NO, which were elevated during the morning hours, often dropped below 500 pptv during the afternoon. The daytime emissions of NO_x that were recorded during the project displayed a rapid increase at 05:00 and then remained reasonably constant throughout the day, with a mean flux value of 4.6 mg m^{-2} hr^{-1}, before dropping again at 17:00 (Squires et al., 2020). The rapid decrease in NO into the afternoon, therefore, was not driven by a change in emissions, but rather instead by the increasing boundary layer depth and also by the chemistry, as elevated levels of ozone observed in the afternoon effectively titrated NO to NO_2 (Newland et al., 2020). Isoprene mixing ratios also peaked in the afternoon, often reaching a few ppbv, indicative of a biogenic source. The variation in NO_x and VOC concentrations experienced at the site provides an opportunity to assess the skill of the MCM to capture the complex chemistry occurring over an extremely wide range of chemical regimes that encompasses both typical urban conditions (high NO_x) as well as chemical conditions more akin to forested environments (low NO, high BVOC). From the 9th – 12th June, NO levels were elevated throughout the day suggesting a local source, whilst from the 17th June to the end of the measurement period, NO concentrations dropped and, so as well as the strong diurnal trend observed in the NO concentration, these periods provide further opportunity to test the model's ability to predict radical concentrations as a function of NO by removing concomitant variables such as changing boundary layer depth and sunrise which occurred in unison with the morning increase in NO concentration.

3.2 Radical concentrations and OH reactivity

The concentrations of RO_x ($OH + HO_2 + RO_2$) radicals were high during the campaign (Figure 2), with OH concentrations frequently exceeded 1 x 10^7 molecule cm^{-3} and reaching up to 2.8 x 10^7 molecule cm^{-3} on the 30th May. These OH levels are amongst the highest measured in an urban environment (Lu et al., 2019), and are comparable to the OH concentrations observed in the Pearl River Delta downwind of the Southern Chinese megacity of Guangzhou, where OH concentrations reached 2.6 x 10^7 molecule cm^{-3} (Lu et al., 2012). HO_2 concentrations peaked at 1 x 10^9 molecule cm^{-3} on the 9th June, whist the highest concentrations of total RO_2 were observed during the latter half of the campaign, peaking at 5.5 x 10^9 molecule cm^{-3} on the afternoon of the 15th June. RO_2 measurements, alongside OH and HO_2, were, until recently, relatively rare. OH and RO_x were measured during the MEGAPOLI project in Paris (Michoud et al., 2012) where the average daytime maximum concentrations of RO_x were 1.2 x 10^8 molecule cm^{-3} which is over an order of magnitude lower than the levels observed in Beijing. Since the development of the RO_xLIF technique, (Fuchs et al., 2008), RO_2 observations are now reported by the Leeds, Juelich and PKU FAGE groups. RO_2 concentrations observed in London in the summer reached up to 5.5 x 10^8 molecule cm^{-3} in air masses that had previously passed over central London (Whalley et al., 2018). In Wangdu, a town situated on the North China Plain, 170 km northeast of Beijing, summertime RO_2 concentrations reached up to 1.5 x 10^9 molecule cm^{-3} (Tan et al., 2017) which, although lower than observed in central Beijing, are much higher than observed in the summertime in European cities suggesting that there may be significant differences in the urban photochemistry occurring in China and Europe.

As well as the elevated daytime radical concentrations, concentrations of OH, HO_2 and RO_2 remained elevated above the instrumental LOD on most nights. The high night-time OH concentrations (ranging from the LOD up to 2 x 10^6 molecule cm^{-3}) are comparable to the levels of OH observed at night in Yufa (a suburb of Beijing) and downwind of Guangzhou where night-time OH concentrations ranged from 0.5 – 3 x 10^6 molecule cm^{-3} (Lu et al., 2014). The observations of OH from the earlier China campaigns could be reconciled by a model if an additional RO_x production process was included which recycled RO_2 to OH via HO_2. A weak positive correlation is observed between night-time OH and RO_2 at night during AIRPRO and the secondary peak in RO_2 occurred when NO_3 was observed to increase rapidly at ~19:30 suggesting that nitrate chemistry was one source of radicals in the evening. Alkyl nitrates, formed from ~~aldehydes~~ isoprene + NO_3 were also enhanced at these times at this site (Reeves et al., 2019).

The OH reactivity, typical of urban environments displayed an inverse relationship with boundary layer height and was highest during the nights when emissions were compressed into a lower boundary layer depth of ~150 m. An average maximum of k(OH) ~37 s^{-1} was observed at 06:00 with OH reactivity reaching 89 s^{-1} on the 15th June at 03:00. During the daytime the OH reactivity dropped to a minimum of ~22 s^{-1} on average at ~15:00 when the boundary layer had increased to ~1500 m. The magnitude of OH reactivity observed during AIRPRO is comparable to the OH reactivity observed at other urban sites in China in the summer (Lou et al., 2010; Fuchs et al., 2017) and also in Tokyo during the summer (Sadanaga et al., 2004; Chatani et al., 2009). In London, OH reactivity was approximately ~7 – 10 s^{-1} lower than in central Beijing with ~15 s^{-1} observed during the day on average and an average maximum of ~27 s^{-1} at 06:00 (Whalley et al., 2016). Lower OH reactivities are also reported from US urban sites in New York and Texas (Ren et al., 2003; Mao et al., 2010).

3.3 Experimental Radical Budget Analysis

Owing to the relatively short-lifetime of radicals, it can be assumed that their production rates and destruction rates are balanced. A comparison of the rates of production and destruction for each radical species can be used to help identify if all radical sources and sinks are accounted for and if the rates of propagation between radical species is fully understood. In London, the ratio of the OH production rate (Eq. 1) to OH destruction rate (Eq.2) was generally close to 1 throughout the campaign demonstrating consistency between the OH, HO_2, k(OH), HONO and NO observations (Whalley et al., 2018). However, under low NO conditions (<0.5 ppbv) the rate of OH destruction exceeded the calculated production rate indicating that Eq.1 was missing a source term under these regimes (Whalley et al., 2018). A steady-state analysis of HO_2 conducted for the London project which balanced the HO_2 production terms (Eq.3) with the first and second order loss terms (Eq.4) highlighted that closure between the production and destruction terms could only be reconciled if the rate of propagation of the observed RO_2 radicals to HO_2 was decreased substantially to just 15%, demonstrating that the mechanism by which RO_2 radicals propagate to other radical species may not be well understood (Whalley et al., 2018). As set out by Tan et al., (2019), analogous budget analyses can be performed for RO_2 species (Eq.5 – Eq.6) and for the entire RO_x budget (Eq.7 – Eq.8). Tan et al., (2019) found that the production and destruction terms for RO_2 were balanced in the mornings in the PRD, when the measured OH reactivity was used to calculate the rate of RO_2 production from VOC+OH reactions, but during the afternoon a missing RO_2 sink (2 – 5 ppbv hr^{-1}) was evident. In the PRD study (Tan et al., 2019), the OH destruction rate exceeded the production rate by 4 – 6 ppbv hr^{-1} in the afternoon, but, in contrast to London (Whalley et al., 2018), the HO_2 budget was closed throughout the whole day. The total rate of RO_x production and destruction were in good agreement in the PRD (Tan et al., 2019).

A comparison of the campaign median production and destruction rates for RO_x, OH, HO_2 and RO_2 during AIRPRO are presented in figure 3. The total rate of RO_x production and destruction are in good agreement throughout the day from ~10 am. A night-time source of radicals of just under 1 ppbv hr^{-1} is missing from the budget analysis likely reflecting missing production from NO_3 +VOC reactions (night-time radical production is considered further in section 3.5). From 6 am to 10 am, the RO_x destruction exceeds the production by up to 4 ppbv hr^{-1} indicating a substantial, ~50%, missing primary RO_x source at this time. Previous work has suggested that Cl-initiated VOC oxidation may be an important source of RO_2 radicals in urban regions (Riedel et al., 2014; Bannan et al., 2015; Tan et al., 2017) but has not been included in the RO_x or RO_2 production rate calculations here. Nitryl chloride was measured for part of the AIRPRO campaign and the impact of this on the modelled RO_2 concentration is investigated in section 3.4. The total RO_x production and destruction rate is of the order of 6 ppbv hr^{-1} at noon which is slightly faster than in the PRD, where a median peak total radical production rate of ~4 ppbv hr^{-1} was calculated. The median OH destruction rate is ~ 30 ppbv hr^{-1} at noon and is roughly twice as fast the production rate at this time highlighting a large missing source of OH radicals in the budget (~ 15 ppbv hr^{-1}). Although a missing OH source was also reported in the PRD (Tan et al., 2019), the missing production rate is ~ 3 times faster during AIRPRO. The known OH production rate during AIRPRO is dominated by the reaction of HO_2 with NO (contributing ~60 % during the day to P(OH) in Eq.1). The median peak HO_2 production of ~60 ppbv hr^{-1} is observed in the morning hours and greatly exceeded the known rate of HO_2 destruction by ~ 50 ppbv hr^{-1}. HO_2 production is driven by the reaction of RO_2 with NO which accounts for 88% of the total. The reaction of OH with CO and HCHO accounts for a further 9%. The total HO_2 production rate is approximately 4 times faster than that calculated for the PRD (Tan et al., 2019). The total rate of RO_2 destruction mirrors the HO_2 production in that it is dominated by the reaction of RO_2 radicals with NO. From sunrise – 14:00 the rate of RO_2 destruction is faster than RO_2 production by up to 50 ppbv hr^{-1}. After 14:00 the rate of RO_2 production and destruction are in good agreement. This trend contrasts with the budget analysis presented from PRD (Tan et al., 2019), which highlighted a possible missing RO_2 sink during the afternoon hours and budget closure in the morning hours.

Binning the ratio of P(OH) to D(OH), P(HO_2) to D(HO_2) and P(RO_2) to D(RO_2) against NO mixing ratio (figure 4) reveals that the RO_2 budget is in good agreement at the lowest NO mixing ratios but as NO mixing ratios increase the destruction of RO_2 becomes faster than production of RO_2 by up to a factor of 10 at the highest NO bin. The trends in the RO_2 and HO_2 ratios are similar in the morning hours, albeit in opposite directions, and suggests that rather than there being a missing primary source of RO_2 and missing sink for HO_2 that happen to balance, instead, as found in London (Whalley et al., 2018), the net propagation rate of RO_2 to HO_2 may be substantially slower than the rate that has currently been used in this analysis. In London (Whalley et al., 2018), the modelled rate of production analysis revealed that only ~50% of the total RO_2 species propagated to HO_2 following reaction with NO, as a significant fraction of the alkoxy radicals formed (such as those generated during the oxidation of monoterpenes and long-chain alkanes) preferentially isomerised and reformed a more oxidised RO_2 species in the presence of O_2 instead. In the London model radical flux analysis using the MCM3.2 , (Whalley et al., 2018), the propagation of alkyl- and acyl-RO_2 species were combined and so the interconversion of acyl-RO_2 radicals (from the OH-initiated oxidation of aldehydic VOCs, photolysis of ketones and decomposition of PAN species) to alkyl-RO_2 radicals following reaction with NO was not explicitly shown, but this interconversion of one RO_2 species to another would serve to reduce the fraction of RO_2 radicals that propagate to HO_2 further. Thus far for AIRPRO, the experimental budget analysis has assumed that 95% of the measured RO_2 species, upon reaction with NO, produce HO_2. If, however, a large fraction of the total RO_2 measured derive from long-chain alkanes, monoterpenes or acyl-RO_2 species, the budget analysis will over-estimate HO_2

production and also the net RO_2 destruction, as the reaction of these peroxy radicals with NO effectively converts one RO_2 species to another RO_2 species, and so the reaction with NO will be neutral in terms of RO_2 production and destruction. Taking $\alpha = 0.1$ leads to a good agreement between the production and destruction rates of HO_2 over the whole day and the observed range of NO. The production and destruction rates of RO_2 agree under high NO conditions, but at NO mixing ratios <5 ppbv the production of RO_2 exceeds the destruction, highlighting (if this α value is correct) that there is a missing RO_2 sink at the lower NO concentrations. Tan et al., (2019) also report a missing RO_2 sink under low NO conditions during PRD and suggested that autoxidation of RO_2 species could account for this missing sink and may also possibly act as the missing source of OH identified under the low NO conditions. An additional first order reaction that converts RO_2 to OH at a rate of 0.1 s^{-1} brings the P:D(OH) and P:D(RO_2) ratios close to 1 at all NO mixing ratios >0.3 ppbv, but at low NO mixing ratios (0.1 – 0.3 ppbv range) an even slower rate of conversion is required, highlighting, as one might expect, that the overall rate of RO_2 isomerisation is variable and likely depends on the specific RO_2 species present at a particular time or location. In the PRD study (Tan et al., 2019), the HO_2 budget was closed when $\alpha = 0.95$ was used suggesting that acyl peroxy radicals and those derived from long-chain alkanes and monoterpenes only made up a very small fraction of the total RO_2 concentration.

Although revealing, this type of experimental budget analysis coupled with the radical observations is unable to differentiate between different RO_2 types and so assumptions have to be made on the fraction of the total RO_2 that propagate to HO_2. In the following section, a box model constrained to the latest MCM scheme (MCM3.3.1) is used to predict the radical concentrations. The MCM is a near explicit model and, as such, treats the production, propagation and destruction of each RO_2 species present discretely and so can provide an insight into the rate at which different RO_2 species convert to HO_2 or to other RO_2 species (or, indeed to OH) and the impact this propagation has on NO to NO_2 conversion and, hence, O_3 production.

3.4 MCM modelled radical predictions and comparison with observations

The time-series of the model-predicted radical concentrations and a breakdown of the modelled OH reactivity from the base MCM model are overlaid with the observations in figure 2. The average diurnal of the measured and modelled radical and k(OH) profiles are also provided in figure 5. In contrast to the experimental budget analysis, the model predicted OH is in excellent agreement with the observed OH throughout the campaign. This same model over-estimates HO_2, however, particularly during the daytime, but also during the evening when a small secondary peak in HO_2 is predicted but not observed. An exception to this trend occurs between the 9^{th} – 12^{th} June when elevated levels of NO were measured at the site during the day and on these days, the agreement between the observed HO_2 and the model is better. The over-prediction of HO_2 primarily occurs under the lower NO conditions that were typically observed during the afternoon hours; the skill of the model to predict the radical concentrations as a function of NO is discussed further below. The model under-estimates total RO_2 throughout the measurement period, although the level of disagreement (in terms of absolute concentration) is most severe from the 16th – 22nd June when NO concentrations were at their lowest. During this period, the average NO mixing ratio was ~0.4 ppbv during the afternoon hours, whilst the average NO mixing ratio for the entirety of the campaign was ~0.75 ppbv during the afternoons

(Fig S1 in SI). The average peak NO mixing ratio observed in the morning (16th – 22nd June) was just over 6 ppbv, whilst the average peak NO mixing ratio for the entirety of the campaign was close to 16 ppbv. ~~The model under-estimates total RO_2 throughout the measurement period, although the level of disagreement (in absolute concentration) is most severe from the 15th – 22nd June when NO concentrations were at their lowest.~~ During this period, the observed RO_2 concentrations were most elevated relative to other times during the campaign, however, the model does not predict a similar increase in RO_2 concentrations during this period relative to other times in the campaign. OH reactivity is under-estimated by the model, on average by ~10 s^{-1}. However, between the 15th – 22nd June the average missing OH reactivity increases to ~ 13 s^{-1}. The model underestimation of OH reactivity may, in part, contribute to the model under-estimation of RO_2 as the model is evidently underestimating the rate of OH + VOC reactions which form RO_2. Including an additional reaction between OH and VOC to account for the missing reactivity in the model and the impact this has on the modelled radical concentrations is investigated in section 3.6. Although the model is able to capture the observed OH concentrations reasonably well, the model's failure to reproduce the observed HO_2 and RO_2 (and in the base model, the OH reactivity) indicates the model is either missing or misrepresenting some key reactions. Furthermore, the discrepancy between the model-predicted OH and OH budget analysis which highlighted a missing OH source, suggests that the over-prediction of HO_2 is masking a missing OH source in the MCM model.

Qualitatively, the model over-estimation of HO_2 and under-estimation of RO_2 is consistent with the budget analysis which identified a missing RO_2 production term and missing HO_2 destruction term which could be reconciled, in part, by slowing the rate at which RO_2 propagate to HO_2. However, when the HO_2 measured to modelled ratio is binned against NO, differences between the model and budget analyses become apparent (figure 6). The model over-predicts the observed HO_2 concentrations at the lowest NO mixing ratios experienced (0.1 – 1 ppbv); this over-prediction can be reconciled (under the very lowest NO conditions, <0.3 ppbv) when a loss of HO_2 to aerosols (calculated using Eq. 9, with an uptake coefficient of 0.2) is included in the model. This demonstrates that a reduction in aerosol surface area has the potential to enhance HO_2 concentrations and thereby increase photochemical ozone formation, but only under very low NO conditions. As there was little to no change in the modelled HO_2 concentration upon inclusion of an heterogeneous loss term under the higher NO conditions, efforts to reduce anthropogenic PM when NO is present (which is highly likely to be the case) would not be expected to lead to an increase in HO_2 and, in turn, O_3 as was suggested from earlier modelling studies (Li et al., 2019). Between 1 – 5 ppbv NO, the model is able to reproduce the observed HO_2 well (between the 9th – 12th June, the daytime NO concentrations fell within this intermediate NO range, hence the good agreement between the model and observations on these days). In contrast with the budget analysis, the model under-predicts HO_2 beyond 5 ppbv NO by up to a factor of 10 at the highest NO experienced (see the 52 ppbv NO bin, figure 6, which includes NO mixing ratios up to 104 ppbv). The model under-predicts the observed RO_2 over the whole NO range and, consistent with the RO_2 budget analysis, the under-prediction (in terms of %) is greatest at the highest NO concentrations experienced during the morning hours. The model under-predicts the observed RO_2 by ~factor of 70 in the highest NO mixing ratio bin-range whereas the destruction rate of RO_2 exceeded the production rate by a factor of ~10 in the budget analysis. This large under-prediction of RO_2 by the model under the highest NO concentrations is most likely driving the differences noted between the P to D(HO_2) and the measured to modelled (HO_2) ratios at NO mixing ratios >5 ppbv. Previous radical studies made at urban sites which were influenced by a range of NO_x concentrations have demonstrated that the level of agreement between model predictions and the observations tends to vary with the level of NO: Models have a tendency to under-predict the observed OH concentrations at NO mixing ratios below 1 ppbv (Lu et al., 2012; Lu et al., 2013; Tan et al., 2017; Whalley et al., 2018) and RO_2 concentrations are increasingly under-predicted as NO concentrations rise (Tan et al., 2017; Whalley et al., 2018; Slater et al., 2020).

Cl atoms, formed from the photolysis of nitryl chloride ($ClNO_2$) have been shown to act as a source of RO_2 (Riedel et al., 2014; Bannan et al., 2015; Tan et al., 2017) and have also been investigated here to see if Cl chemistry can resolve the modelled RO_2 under-prediction under the elevated NO concentrations which were typically observed during the mornings. $ClNO_2$ was measured for part of the campaign (Zhou et al., 2018) and reached up to 1.44 ppbv during the night on the 12th – 13th June. The Cl atom concentration, calculated from the concentration of $ClNO_2$, its photolysis rate to yield Cl (determined from the observed actinic flux and published absorption cross section of $ClNO_2$) and the VOC loading, exceeded 4 x 10^4 atoms cm^{-3} during the morning of the 13th June and exceeded 1 x 10^4 atoms cm^{-3} on several other mornings (figure 7). During these times, the modelled RO_2 concentrations increased, relative to the concentration in the base model, by up to 2.5 x 10^8 molecule cm^{-3} which represents close to a 100% increase in the modelled RO_2 at these times. On several mornings (4th, 5th, 7th and 13th June) this increase in RO_2 brought the model and measured RO_2 into close agreement. The production rate of RO_2 from Cl-initiated VOC oxidation on these mornings would serve to enhance P(RO_x) by up to 2.1 ppbv hr^{-1}~~to the rate of D(RO_x)~~. However, on several nights, only low concentrations of $ClNO_2$ were measured and only very low concentrations of Cl atoms were calculated to be present upon sunrise and so, on these days, only modest enhancements (1 – 2 x 10^7 molecule cm^{-3}) in RO_2 concentrations were predicted by the model and the large under-prediction in the RO_2 concentration on these mornings remained which may indicate that there are other, overlooked, primary RO_x sources in the experimental budget calculation besides missing Cl + VOC reactions. The Cl atom concentration dropped off rapidly during the mornings with just ~100 atoms cm^{-3} present by noon on most days and so was unable to reconcile the magnitude of the RO_2 underestimation observed throughout the day.

3.5 Rate of Production and rate of Destruction analysis

A rate of production and rate of destruction analysis on model OH, HO_2 and RO_2 species (figure 8) highlights the main radical sources and sinks in the base model. Consistent with earlier studies of radicals in urban locations, the photolysis of HONO is the dominant primary source of radicals during the daytime, accounting for ~64 % of the primary radical production on average during the day (05:00 – 19:30) throughout the campaign. The photolysis of O_3 and subsequent reaction of O(^{1}D) with H_2O vapour accounts for ~9 % of primary production during the day, whilst the photolysis of HCHO and other photo-labile VOCs accounts for ~11 % of the radical production. Ozonolysis and nitrate radical (NO_3) reactions account for 9 % and 7 % of the total radical production during the day, respectively. At night, both ozonolysis (~18 %) and nitrate radical reactions (~82 %)

are the source of radicals. The primary source of radicals from VOC+NO_3 reactions is ~ 1 ppbv hr^{-1} during the night which is sufficient to close the RO_x experimental budget (figure 3).

Figure 9 highlights the rates of propagation in the model which transform OH to HO_2 and RO_2, RO_2 to HO_2 and HO_2 back to OH. The rate of propagation is rapid and the secondary source of OH from HO_2 + NO is more than twice as large as the primary production of OH from HONO photolysis. Approximately one third of the OH reacts with CO, O_3 or HCHO to form HO_2, just over one third reacts with VOCs to form RO_2 and just under one third is lost by reaction with NO_2 forming nitric acid. In contrast to London (Whalley et al., 2018), the majority of RO_2 formed during AIRPRO propagate to HO_2 and subsequently the majority of HO_2 propagates back to OH. From the model radical flux analysis, which takes into consideration the different types of RO_2 species present, a value of $\alpha = 0.87$ is derived (where α = 1 minus the rate at which RO forms RO_2 or $RC(O)O_2$ divided by the rate of RO conversion to HO_2). Note, this fraction does not consider RO_2 and $RC(O)O_2$ termination reactions. In London, the model derived α was ~0.5 reflecting the presence of long-chain alkane-derived RO_2 species from diesel emissions and mono-terpenes. In Beijing, measurement of such long-chain VOC species could not be attempted, but these could have been present. A lumped mono-terpene signal was measured by PTR-ToF-MS and is included in the model, split equally between α-pinene and limonene. The base model, on which the radical flux analysis was performed, under-predicts OH reactivity and so is likely missing RO_2 species from additional OH+VOC reactions which, depending on the RO_2 type may serve to reduce α.

3.6 OH reactivity and missing OH reactivity

NO_2 was the single biggest contributor to the OH reactivity in Beijing with a campaign average contribution of 18.6% (figure 5). This is similar to the NO_2 contribution to OH reactivity observed in London (Whalley et al., 2016). NO contributed just 1.3% to the total reactivity in Beijing, compared to a 4.2% contribution in London (Whalley et al., 2016). In London, measured carbonyl species accounted for close to 20% of the OH reactivity budget, largely due to the high concentrations of HCHO (Whalley et al., 2016). In contrast, in Beijing, carbonyls accounted for just 3.8% of the measured k(OH). Alkenes and dialkenes were more prevalent in Beijing than in London and the dialkene group of VOCs (dominated by isoprene) accounted for 10.5% of the OH reactivity in Beijing compared to 1.8% in London (Whalley et al., 2016). Owing to the faster physical loss of secondary species in Beijing by ventilation compared to London (see section 2), the contribution that model-generated intermediate species made to the observed OH reactivity was 2.7% in Beijing vs 23.8% in London (Whalley et al., 2016). In contrast to Beijing, where approximately 30% of the measured reactivity remains unaccounted for, in London, the OH reactivity budget was largely closed (Whalley et al., 2016). In Beijing during the measurement period when the missing OH reactivity reached on average 13 s^{-1} (15th – 22nd June), isoprene concentrations were elevated relative to earlier in the campaign (figure 1). Overall, much higher concentrations of isoprene were observed in Beijing than in London (Whalley et al., 2016), and so this may indicate that other biogenic species that were not measured, along with their oxidation products, may account for some of the missing OH reactivity in Beijing.

A series of model simulations have been performed where an additional OH to RO_2 reaction has been included to account for the missing reactivity at a given time (figure 10); the RO_2 formed has been varied to investigate the influence of different RO_2 types on the modelled radical concentrations. When OH converts to methyl peroxy radicals, the modelled RO_2 concentration increases by close to a factor of 2 on average, but just over a factor of 2 under-prediction of the observed RO_2 radicals remains. Unsurprisingly, it is the modelled fraction of RO_2 radicals that do not act as an HO_2 interference (RO_2-simple) that increase in this scenario and the model now only under-estimates this class of RO_2 species by a factor of 1.45, whilst RO_2-complex is still under-estimated by a factor of 6.2. When OH converts to $HOCH_2CH_2O_2$ (an RO_2 species that does act as an HO_2 interference, formed from the reaction of OH with ethene), the modelled RO_2-complex fraction increases and the model under-estimation of RO_2-complex is reduced to a factor of 1.8 on average, with the largest under-predictions observed during the evening hours. In both these model simulations, the modelled over-prediction of HO_2 increases from the base model scenario as CH_3O_2 and $HOCH_2CH_2O_2$ both rapidly propagate to HO_2. The modelled OH concentration displays a modest decrease with the additional OH sink, however, this is largely compensated for by the increase in modelled HO_2 which enhances the secondary source of OH from HO_2 + NO, and so, overall, the modelled OH concentration is largely buffered by the inclusion of missing OH reactivity in the form of additional methane (leading to CH_3O_2) or ethene (leading to $HOCH_2CH_2O_2$)

Model simulations (not shown) which include an additional source of $CH_3C(O)O_2$, for example, from additional CH_3CHO+OH reactions, do predict substantially less HO_2 (and can reconcile the observed HO_2 to with 25%), but modelled RO_2 concentrations do not increase as a large fraction of the acyl-RO_2 radicals react with NO_2 to form PAN and are, therefore, lost. These missing reactivity model simulations and measurement comparisons suggest that the missing RO_2 may be a species which, upon reaction with NO, converts from one RO_2 species to another and, therefore, compete with RO_2 to HO_2 propagation rather than a RO_2 radical which lead to RO_2 termination. This suggests that the overall lifetime of RO_2 radicals is longer than currently estimated and that multiple conversions of one RO_2 species to another may be occurring to sustain the high concentrations observed. As identified in London, larger, more complex VOC species such as mono-terpenes or long-chain alkanes deriving from diesel emissions do undergo multiple RO_2 to RO_2 conversions in the presence of NO as the alkoxy radical formed preferentially undergoes isomerisation rather than an external H atom abstraction by O_2. If an additional reaction which converts OH to an RO_2 species formed during the oxidation of α-pinene, and which undergoes four reactions with NO before eventually forming HO_2, is added to the model at a rate sufficient to reconcile the missing OH reactivity, the model predicts significantly more total RO_2 and now only modestly under-predicts the observed RO_2 concentrations (by a factor of 1.8). The modelled radical concentrations predicted from the 'Missing k(OH) (OH to C96O2)' scenario are overlaid with the radical observations and modelled radicals from the base model scenario in Fig S2, SI. The additional VOC reactivity which produces RO_2 radicals that isomerise after reaction with NO is able to increase the modelled total RO_2 concentration both under the lower NO conditions experienced between the 16th – 22nd June as well as on the higher NO days 9th – 12th June indicating that NO is still at sufficient concentrations to dominate the fate of RO_2 between the 16th – 22nd June, despite NO concentrations being lower. The median measured to modelled (Missing k(OH) (OH to C96O2)) ratio vs NO (Fig S3, SI) highlights that the inclusion of alkoxy isomerisation following RO_2 + NO reaction increases the modelled RO_2 across the entire NO range but, considering the log scale, has the biggest impact on the ratio (from the measured to modelled (base) ratio) at the highest NO concentration. ~~In this simulation, b~~Both the simple- and complex-RO_2 species are enhanced, as the first 3 generations of RO_2 species formed would be detected during the RO_x-mode in the RO_x-LIF instrument and, hence, contribute to RO_2-simple. The final RO_2 species formed, that does propagate to HO_2 via RO upon reaction with NO, would be detected during the HO_x-mode in the RO_xLIF instrument and, as such, contributes to the RO_2-complex fraction. In this scenario, the HO_2 concentration is now only modestly over-estimated by a factor of 1.4. The RO_xLIF instrument relies on the conversion of RO_2 species to HO_2 (and ultimately to OH) for detection, so one might expect the instrument to be insensitive to RO_2 species that do not directly propagate to RO then to HO_2 upon reaction with NO. However, given the RO_xLIF flow tube conditions (NO concentration of 4 x 10^{13} molecule cm^{-3} and residence time of just under 1 s) RO_2 species that require several reactions with NO before HO_2 is produced should still be detected. These types of RO_2 species that require more than one reaction with NO before HO_2 forms may be generated via the additional VOC+OH reactions identified as missing OH reactivity (as presented here). They may also be present due to a missing primary source of RO_2 such as decomposition of a complex PAN species, VOC photolysis, a Cl atom + VOC reaction or an alkene ozonolysis product. The experimental peroxy radical budget analysis highlighted that budget closure could only be achieved if α was reduced to 0.1, which suggests that the model breakdown of peroxy radical species present (e.g. the fraction of acyl-RO_2, long- vs short-chained alkyl-RO_2 species) may be incomplete. In the scenario where OH converts to an α-pinene-derived RO_2 species, consistent with the experimental budget analysis, the model under-predicts the observed OH by a factor of 1.8 revealing that there is a missing source of OH under the low NO conditions in Beijing that was previously masked by the model over-prediction of HO_2.

3.7 Impact on ozone production

Previous work, for example, by Tan et al (2017), suggested that the addition of a primary RO_2 source could help reconcile the model under-prediction of RO_2. However, as demonstrated in section 3.6, the identity of the primary RO_2 is important and in Beijing a complex RO_2 species that has a large enough carbon skeleton such that the RO radical formed upon reaction with NO preferentially isomerises to another RO_2 (and undergoes multiple RO_2 to RO_2 conversions before *eventually* forming HO_2) is needed to reconcile both the observed RO_2 and HO_2 concentrations. These types of RO_2 species may also preferentially isomerise rather than undergo the bimolecular reactions with NO if NO concentrations are low enough. For example, laboratory studies have shown that the monoterpenes, following an initial attack by ozone or OH, form highly oxidised RO_2 radicals within a few seconds via repeated H-shift from C– H to an R–O–O bond and subsequent O_2 additions (Jokinen et al., 2014; Ehn et al., 2014; Berndt et al., 2016). Recently, autoxidation has also been shown to occur during the oxidation of aromatic VOCs too (Wang et al., 2017b). Autoxidation reactions may generate OH directly from RO_2 and, therefore, may also resolve the missing OH source reported under low NO conditions (here and in the literature). These types of autoxidation reactions lead to the generation of HOMs also which have been shown to condense and contribute to SOA (Mohr et al., 2019). Mass spectrometric signals relating to these highly oxidised RO_2 species were observed during the AIRPRO campaign (Brean et al., 2019; Mehra et al., 2020) suggesting that autoxidation was occurring at the Beijing site. Unimolecular H-atom shifts are represented within the MCM3.3.1 for isoprene oxidation. Autoxidation reactions for other RO_2 radicals are currently not included within the MCM3.3.1, although improved representation of RO_2 radical chemistry is a focus for the next generation of explicit detailed chemical mechanisms (Jenkin et al., 2019). In addition to missing unimolecular RO_2 reactions, the model may be missing other RO_2 reaction pathways, for example, RO_2 accretion reactions, as identified by Berndt et al (2018). Although it is difficult to fully assess how competitive these RO_2+RO_2 reactions may be compared to RO_2+NO reactions from the total RO_2 observations made (the concentration of each individual RO_2 would be needed), the inclusion of accretion reactions in the MCM would serve to reduce the modelled RO_2 concentration under low NO_x conditions as the reaction represents an overall RO_x sink. This suggests that the missing RO_2 source identified here may be even larger under the lower NO conditions.

The model measurement comparisons above suggest that our understanding of the rate at which the larger RO_2 species propagate to HO_2 (or to OH directly) and the possible reactions they undergo (which have not undergone substantial laboratory study) is far from complete and highlights that RO_2 chemistry warrants further study. One important finding, however, is that the underestimation of the observed RO_2 may be caused by missing reactions that compete with the RO_2+NO reactions that form HO_2. These competing reactions are effectively slowing the rate at which RO_2 species convert to HO_2, but if, as suggested here, these reactions are RO_2+NO reactions that reform another RO_2 radical, they will still be relevant in terms of ozone production. Under low NO conditions there is emerging evidence that unimolecular isomerisation reactions occur for a range of RO_2 radicals (Jokinen et al., 2014; Ehn et al., 2014; Berndt et al., 2016; Wang et al., 2017b)~~; these reactions will effectively remove RO_2 radicals without conversion of NO to NO_2 and so also have implications for modelling in situ O_3 production, if models rely only on the rate of VOC oxidation when investigating O_3 production.~~as well as RO_2 accretion reactions (Berndt et al., 2018). These reactions will effectively remove RO_2 radicals without conversion of NO to NO_2 and so also have implications for modelling in situ O_3 production, if models rely only on the rate of VOC oxidation when investigating O_3 production.

By approximating the rate of ozone production to the rate of NO_2 production from the reaction of NO with HO_2 and RO_2 radicals, urban radical measurements can be used to estimate chemical ozone formation (Kanaya et al., 2007; Ren et al., 2013; Brune et al., 2016; Tan et al., 2017; Whalley et al., 2018). ~~By approximating the rate of ozone production to the rate of NO_2 production from the reaction of NO with HO_2 and RO_2 radicals, urban radical measurements can be used to estimate local~~

~~ozone formation (Kanaya et al., 2007; Ren et al., 2013; Brune et al., 2016; Tan et al., 2017; Whalley et al., 2018). Losses of NO_2 that do not yield O_3, for example through nitric acid and PAN formation, need to be estimated and then subtracted:~~

$$P(\mathrm{O}_{\mathrm{x}\cancel{3}}) = \left(k_{\mathrm{HO_2+NO}}[\mathrm{HO_2}][\mathrm{NO}] + k_{\mathrm{RO_2+NO}}[\mathrm{RO_2}][\mathrm{NO}]\right) \cancel{- \left(k_{\mathrm{OH+NO_2+M}}[\mathrm{OH}][\mathrm{NO_2}][\mathrm{M}] + k_{\mathrm{RO_2+NO_2+M}}[\mathrm{RO_2}][\mathrm{NO_2}][\mathrm{M}]\right)} \tag{11}$$

Losses of O_x ($L(O_x)$) include chemical losses such as the reaction of NO_2 with OH, net PAN formation, the fraction of $O(^1D)$ (formed by the photolysis of O_3) that react with H_2O and the reaction of O_3 with OH and HO_2. Physical loss processes, such as O_3 deposition and ventilation out of the model box (see section 2.4) will also contribute to $L(O_x)$. Physical processes such as advection of O_3 into the model box would also need to be considered in the model to make a direct comparison to the observed O_3 concentrations.

Considering the chemical production of O_x (Eq.11), recent studies where OH, HO_2 and RO_2 observations (via RO_xLIF) were made, demonstrated that models may under-predict ozone production at high NO due to an underestimation of the RO_2 radical concentrations at high NO concentrations (Tan et al., 2017; Whalley et al., 2018).

~~Using this approach, recent studies where OH, HO_2 and RO_2 observations (via RO_xLIF) were made, demonstrated that models may under-predict ozone production at high NO due to an underestimation of the RO_2 radical concentrations at high NO concentrations (Tan et al., 2017; Whalley et al., 2018).~~ Figure 11 displays the mean ozone production calculated from the radical observations (red line) as a function of NO and, consistent with the earlier ozone production calculations from the Wangdu (Tan et al., 2017) and London (Whalley et al., 2018) studies, the in situ ozone production calculated from the modelled OH and peroxy radicals (black line) is lower than from the observed radicals, most significantly at the higher NO concentrations. To accurately simulate ozone production and to understand how emission reduction policies may impact ozone levels, it is essential that the model accurately reflects the types of RO_2 species present and how fast they propagate to another RO_2 species, or to HO_2 or to OH.

4~~5~~ Conclusions

Measurement and model comparisons of OH, HO_2, RO_2-complex, RO_2-simple and total RO_2 in Beijing have displayed varying levels of agreement as a function of NO_x. Under low NO conditions, consistent with previous studies in low NO_x but high VOC environments, a missing OH source is evident. Radical budget analysis has demonstrated that this missing OH source could be resolved if unimolecular reactions of RO_2 radicals generate OH directly. Under the low NO conditions (< 1 ppbv), the MCM over-predicted HO_2, although this over-prediction could be resolved at very low NO mixing ratios (<0.3 ppbv) by including a heterogeneous loss term to aerosol surfaces. This highlights that a reduction in aerosol surface area has the potential to enhance HO_2 concentrations and thereby increase photochemical ozone formation, but only under very low NO conditions.

The model under-predicted RO_2, most severely under high NO conditions (>1 ppbv). Although Cl atoms could increase the concentration of RO_2, this enhancement was limited to times when the Cl atom concentration was elevated and could not resolve the RO_2 under-prediction observed at all times. In the presence of NO, the model over-estimates the rate at which RO_2 propagates to HO_2 and we hypothesise that larger RO_2 species likely undergo multiple bimolecular reactions with NO, followed by isomerisation of the RO radical to another RO_2 species, before a HO_2 radical forms. By this process, the lifetime and the concentration of total-RO_2 radicals is extended. The ozone production efficiency of large, complex VOCs from which these RO_2 species are formed may be greater than currently appreciated, and so further efforts to understand the rate at which the larger RO_2 species propagate to HO_2 (or to OH directly) and all the possible reactions they undergo, is necessary to accurately model ozone levels in urban centres such as Beijing and to fully understand how emission controls will impact ozone.

Data availability. Data presented in this study are available from the author upon request (l.k.whalley@leeds.ac.uk).

Author contributions. LW, ES, RWM, CY and DH carried out the measurements; LW and ES developed the model and performed the calculations; JL, FS, JH, RD, MS, JH, AL, AM, SW, AB, TB, HC, BO, RJ, LC, LK, WB, TV, SK, SG, YS, WX, SY, LR, WA, CH, XW and PF provided logistical support and supporting data to constrain the model; LW prepared the manuscript, with contributions from all the co-authors.

Competing interests. The authors declare that they have no conflict of interest.

Acknowledgements – We are grateful to the Natural Environment Research Council for funding via the Newton Fund Atmospheric Pollution and Human Health in Chinese Megacity Directed International Program (grant number NE/N006895/1) and the National Natural Science Foundation of China (Grant No.41571130031). Eloise Slater, Freya Squires and Archit Mehra acknowledge NERC SPHERES PhD studentships. We would like to thank Likun Xue and co-authors for the providing the chlorine chemistry module used in the MCM. We acknowledge the support from Zifa Wang and Jie Li from the Institute of Applied Physics (IAP), Chinese Academy of Sciences for hosting the APHH-Beijing campaign. We thank Liangfang Wei, Hong Ren, Qiaorong Xie, Wanyu Zhao, Linjie Li, Ping Li, Shengjie Hou and Qingqing Wang from IAP, Kebin He and

Xiaoting Cheng from Tsinghua University, and James Allan from the University of Manchester for providing logistic and scientific support for the field campaigns. We would also like to thank other participants in the APHH field campaign.

References

Bannan, T. J., Booth, A. M., Bacak, A., Muller, J. B. A., Leather, K. E., Le Breton, M., Jones, B., Young, D., Coe, H., Allan, J., Visser, S., Slowik, J. G., Furger, M., Prevot, A. S. H., Lee, J., Dunmore, R. E., Hopkins, J. R., Hamilton, J. F., Lewis, A. C., Whalley, L. K., Sharp, T., Stone, D., Heard, D. E., Fleming, Z. L., Leigh, R., Shallcross, D. E., and Percival, C. J.: The first UK measurements of nitryl chloride using a chemical ionization mass spectrometer in central London in the summer of 2012, and an investigation of the role of Cl atom oxidation, J Geophys Res-Atmos, 120, 5638-5657, 10.1002/2014JD022629, 2015.

Berndt, T., Richters, S., Jokinen, T., Hyttinen, N., Kurten, T., Otkjaer, R. V., Kjaergaard, H. G., Stratmann, F., Herrmann, H., Sipila, M., Kulmala, M., and Ehn, M.: Hydroxyl radical-induced formation of highly oxidized organic compounds, Nat Commun, 7, Artn 13677 10.1038/Ncomms13677, 2016.

Berndt, T., Mentler, B., Scholz, W., Fischer, L., Herrmann, H., Kulmala, M., and Hansel, A.: Accretion product formation from ozonolysis and OH radical reaction of α-pinene: Mechanistic insight and the influence of isoprene and ethylene, Environ. Sci. Tech., 52, 11069-11077, 2018.

Bigi, A., and Harrison, R. M.: Analysis of the air pollution climate at a central urban background site, Atmos Environ, 44, 2004-2012, 10.1016/j.atmosenv.2010.02.028, 2010.

Brean, J., Harrison, R. M., Shi, Z. B., Beddows, D. C. S., Acton, W. J. F., Hewitt, C. N., Squires, F. A., and Lee, J.: Observations of highly oxidized molecules and particle nucleation in the atmosphere of Beijing, Atmos Chem Phys, 19, 14933-14947, 10.5194/acp-19-14933-2019, 2019.

Brune, W. H., Baier, B. C., Thomas, J., Ren, X., Cohen, R. C., Pusede, S. E., Browne, E. C., Goldstein, A. H., Gentner, D. R., Keutsch, F. N., Thornton, J. A., Harrold, S., Lopez-Hilfiker, F. D., and Wennberg, P. O.: Ozone production chemistry in the presence of urban plumes, Faraday Discuss, 189, 169-189, 10.1039/c5fd00204d, 2016.

Chatani, S., Shimo, N., Matsunaga, S., Kajii, Y., Kato, S., Nakashima, Y., Miyazaki, K., Ishii, K., and Ueno, H.: Sensitivity analyses of OH missing sinks over Tokyo metropolitan area in the summer of 2007, Atmos Chem Phys, 9, 8975-8986, DOI 10.5194/acp-9-8975-2009, 2009.

Chen, R. J., Zhao, Z. H., and Kan, H. D.: Heavy Smog and Hospital Visits in Beijing, China, Am J Resp Crit Care, 188, 1170-1171, DOI 10.1164/rccm.201304-0678LE, 2013.

Commane, R., Floquet, C. F. A., Ingham, T., Stone, D., Evans, M. J., and Heard, D. E.: Observations of OH and HO2 radicals over West Africa, Atmos Chem Phys, 10, 8783-8801, 10.5194/acp-10-8783-2010, 2010.

Crilley, L. R., Kramer, L. J., Ouyang, B., Duan, J., Zhang, W. Q., Tong, S. R., Ge, M. F., Tang, K., Qin, M., Xe, P. H., Shaw, M., Lewis, A. C., Mehra, A., Bannan, T. J., Worrall, S. D., Priestley, M., Bacak, A., Coe, H., Allan, J., Percival, C. J., Popoola, O. A. M., Jones, R. L., and Bloss, W. J.: Intercomparison of nitrous acid (HONO) measurement techniques in a megacity (Beijing), Atmos Meas Tech, 12, 6449-6463, 10.5194/amt-12-6449-2019, 2019.

Cryer, D. R.: Measurements of hydroxyl radical reactivity and formaldehyde in the atmosphere, PhD, School of Chemistry, University of Leeds, UK, 2016.

Ehn, M., Thornton, J. A., Kleist, E., Sipila, M., Junninen, H., Pullinen, I., Springer, M., Rubach, F., Tillmann, R., Lee, B., Lopez-Hilfiker, F., Andres, S., Acir, I. H., Rissanen, M., Jokinen, T., Schobesberger, S., Kangasluoma, J., Kontkanen, J., Nieminen, T., Kurten, T., Nielsen, L. B., Jorgensen, S., Kjaergaard, H. G., Canagaratna, M., Dal Maso, M., Berndt, T., Petaja, T., Wahner, A., Kerminen, V. M., Kulmala, M., Worsnop, D. R., Wildt, J., and Mentel, T. F.: A large source of low-volatility secondary organic aerosol, Nature, 506, 476-+, 10.1038/nature13032, 2014.

Fuchs, H., Holland, F., and Hofzumahaus, A.: Measurement of tropospheric RO2 and HO2 radicals by a laser-induced fluorescence instrument, Rev Sci Instrum, 79, Artn 084104 10.1063/1.2968712, 2008.

Fuchs, H., Tan, Z. F., Lu, K. D., Bohn, B., Broch, S., Brown, S. S., Dong, H. B., Gomm, S., Haseler, R., He, L. Y., Hofzumahaus, A., Holland, F., Li, X., Liu, Y., Lu, S. H., Min, K. E., Rohrer, F., Shao, M., Wang, B. L., Wang, M., Wu, Y. S., Zeng, L. M., Zhang, Y. S., Wahner, A., and Zhang, Y. H.: OH reactivity at a rural site (Wangdu) in the North China Plain: contributions from OH reactants and experimental OH budget, Atmos Chem Phys, 17, 645-661, 10.5194/acp-17-645-2017, 2017.

He, H., Liang, X. Z., Sun, C., Tao, Z. N., and Tong, D. Q.: The long-term trend and production sensitivity change in the US ozone pollution from observations and model simulations, Atmos Chem Phys, 20, 3191-3208, 10.5194/acp-20-3191-2020, 2020.

Hofzumahaus, A., Rohrer, F., Lu, K. D., Bohn, B., Brauers, T., Chang, C. C., Fuchs, H., Holland, F., Kita, K., Kondo, Y., Li, X., Lou, S. R., Shao, M., Zeng, L. M., Wahner, A., and Zhang, Y. H.: Amplified Trace Gas Removal in the Troposphere, Science, 324, 1702-1704, 10.1126/science.1164566, 2009.

Hopkins, J. R., Jones, C. E., and Lewis, A. C.: A dual channel gas chromatograph for atmospheric analysis of volatile organic compounds including oxygenated and monoterpene compounds, Journal of Environmental Monitoring, 13, 2268-2276, 2011.

Huang, J., Pan, X. C., Guo, X. B., and Li, G. X.: Health impact of China's Air Pollution Prevention and Control Action Plan: an analysis of national air quality monitoring and mortality data, Lancet Planet Health, 2, E313-E323, Doi 10.1016/S2542-5196(18)30141-4, 2018.

Huang, R. J., Zhang, Y. L., Bozzetti, C., Ho, K. F., Cao, J. J., Han, Y. M., Daellenbach, K. R., Slowik, J. G., Platt, S. M., Canonaco, F., Zotter, P., Wolf, R., Pieber, S. M., Bruns, E. A., Crippa, M., Ciarelli, G., Piazzalunga, A., Schwikowski, M., Abbaszade, G., Schnelle-Kreis, J., Zimmermann, R., An, Z. S., Szidat, S., Baltensperger, U., El Haddad, I., and Prevot, A. S. H.: High secondary aerosol contribution to particulate pollution during haze events in China, Nature, 514, 218-222, 10.1038/nature13774, 2014.

Huang, Z., Zhang, Y., Yan, Q., Zhang, Z., and Wang, X.: Real-time monitoring of respiratory absorption factors of volatile organic compounds in ambient air by proton transfer reaction time-of-flight mass spectrometry, Journal of hazardous materials, 320, 547-555, 2016.

Jacob, D. J.: Heterogeneous chemistry and tropospheric ozone, Atmos Environ, 34, 2131-2159, Doi 10.1016/S1352-2310(99)00462-8, 2000.

Jenkin, M. E., Young, J. C., and Rickard, A. R.: The MCM v3.3.1 degradation scheme for isoprene, Atmos Chem Phys, 15, 11433-11459, 10.5194/acp-15-11433-2015, 2015.

Jenkin, M. E., Valorso, R., Aumont, B., and Rickard, A. R.: Estimation of rate coefficients and branching ratios for reactions of organic peroxy radicals for use in automated mechanism construction, Atmos Chem Phys, 19, 7691-7717, 10.5194/acp-19-7691-2019, 2019.

Jokinen, T., Sipila, M., Richters, S., Kerminen, V. M., Paasonen, P., Stratmann, F., Worsnop, D., Kulmala, M., Ehn, M., Herrmann, H., and Berndt, T.: Rapid Autoxidation Forms Highly Oxidized RO2 Radicals in the Atmosphere, Angew Chem Int Edit, 53, 14596-14600, 10.1002/anie.201408566, 2014.

Kanaya, Y., Cao, R. Q., Akimoto, H., Fukuda, M., Komazaki, Y., Yokouchi, Y., Koike, M., Tanimoto, H., Takegawa, N., and Kondo, Y.: Urban photochemistry in central Tokyo: 1. Observed and modeled OH and HO2 radical concentrations during the winter and summer of 2004, J Geophys Res-Atmos, 112, Artn D21312 10.1029/2007jd008670, 2007.

Li, K., Jacob, D. J., Liao, H., Shen, L., Zhang, Q., and Bates, K. H.: Anthropogenic drivers of 2013-2017 trends in summer surface ozone in China, P Natl Acad Sci USA, 116, 422-427, 10.1073/pnas.1812168116, 2019.

Lou, S., Holland, F., Rohrer, F., Lu, K., Bohn, B., Brauers, T., Chang, C. C., Fuchs, H., Haseler, R., Kita, K., Kondo, Y., Li, X., Shao, M., Zeng, L., Wahner, A., Zhang, Y., Wang, W., and Hofzumahaus, A.: Atmospheric OH reactivities in the Pearl River Delta - China in summer 2006: measurement and model results, Atmos Chem Phys, 10, 11243-11260, 10.5194/acp-10-11243-2010, 2010.

Lu, K. D., Rohrer, F., Holland, F., Fuchs, H., Bohn, B., Brauers, T., Chang, C. C., Haseler, R., Hu, M., Kita, K., Kondo, Y., Li, X., Lou, S. R., Nehr, S., Shao, M., Zeng, L. M., Wahner, A., Zhang, Y. H., and Hofzumahaus, A.: Observation and modelling of OH and HO2 concentrations in the Pearl River Delta 2006: a missing OH source in a VOC rich atmosphere, Atmos Chem Phys, 12, 1541-1569, 10.5194/acp-12-1541-2012, 2012.

Lu, K. D., Hofzumahaus, A., Holland, F., Bohn, B., Brauers, T., Fuchs, H., Hu, M., Haseler, R., Kita, K., Kondo, Y., Li, X., Lou, S. R., Oebel, A., Shao, M., Zeng, L. M., Wahner, A., Zhu, T., Zhang, Y. H., and Rohrer, F.: Missing OH source in a suburban environment near Beijing: observed and modelled OH and HO2 concentrations in summer 2006, Atmos Chem Phys, 13, 1057-1080, 10.5194/acp-13-1057-2013, 2013.

Lu, K. D., Rohrer, F., Holland, F., Fuchs, H., Brauers, T., Oebel, A., Dlugi, R., Hu, M., Li, X., Lou, S. R., Shao, M., Zhu, T., Wahner, A., Zhang, Y. H., and Hofzumahaus, A.: Nighttime observation and chemistry of HOx in the Pearl River Delta and Beijing in summer 2006, Atmos Chem Phys, 14, 4979-4999, 10.5194/acp-14-4979-2014, 2014.

Lu, K. D., Guo, S., Tan, Z. F., Wang, H. C., Shang, D. J., Liu, Y. H., Li, X., Wu, Z. J., Hu, M., and Zhang, Y. H.: Exploring atmospheric free-radical chemistry in China: the self-cleansing capacity and the formation of secondary air pollution, Natl Sci Rev, 6, 579-594, 10.1093/nsr/nwy073, 2019.

Mao, J. Q., Ren, X. R., Chen, S. A., Brune, W. H., Chen, Z., Martinez, M., Harder, H., Lefer, B., Rappengluck, B., Flynn, J., and Leuchner, M.: Atmospheric oxidation capacity in the summer of Houston 2006: Comparison with summer measurements in other metropolitan studies, Atmos Environ, 44, 4107-4115, 10.1016/j.atmosenv.2009.01.013, 2010.

Martinez, M., Harder, H., Kovacs, T. A., Simpas, J. B., Bassis, J., Lesher, R., Brune, W. H., Frost, G. J., Williams, E. J., Stroud, C. A., Jobson, B. T., Roberts, J. M., Hall, S. R., Shetter, R. E., Wert, B., Fried, A., Alicke, B., Stutz, J., Young, V. L., White, A. B., and Zamora, R. J.: OH and HO2 concentrations, sources, and loss rates during the Southern Oxidants Study in Nashville, Tennessee, summer 1999, J Geophys Res-Atmos, 108, Artn 4617 10.1029/2003jd003551, 2003.

Mehra, A., Canagaratna, M., Bannan, T., Worrall, S. D., Bacak, A., Priestley, M., Zhao, J., Xu, W., Wang, Y., Cheng, X., Wang, L., Hamilton, J., Chen, Q., Stark, H., Krechmer, J. E., Squires, F. A., Lee, J., Brean, J., Slater, E. J., Whalley, L. K., Heard, D. E., Ouyang, B., Acton, W. J., Hewitt, C. N., Wang, X., Liu, D., Jayne, J. T., Sun, Y., Fu, P., Worsnop, D., Allan, J., Percival, C., and Coe, H.: Using highly time-resolved online mass spectrometry to examine biogenic and anthropogenic contributions to organic aerosol in Beijing Faraday Discuss, 2020.

Michoud, V., Kukui, A., Camredon, M., Colomb, A., Borbon, A., Miet, K., Aumont, B., Beekmann, M., Durand-Jolibois, R., Perrier, S., Zapf, P., Siour, G., Ait-Helal, W., Locoge, N., Sauvage, S., Afif, C., Gros, V., Furger, M., Ancellet, G., and Doussin, J. F.: Radical budget analysis in a suburban European site during the MEGAPOLI summer field campaign, Atmos Chem Phys, 12, 11951-11974, 10.5194/acp-12-11951-2012, 2012.

Mohr, C., Thornton, J. A., Heitto, A., Lopez-Hilfiker, F. D., Lutz, A., Riipinen, I., Hong, J., Donahue, N. M., Hallquist, M., Petaja, T., Kulmala, M., and Yli-Juuti, T.: Molecular identification of organic vapors driving atmospheric nanoparticle growth, Nat Commun, 10, Artn 4442 10.1038/S41467-019-12473-2, 2019.

Newland, M. J., Bryant, D. J., Dunmore, R., Bannan, T., Acton, W. J., Langford, B., Hopkins, J., Squires, F. A., Dixon, W. J., Drysdale, W. S., Ivatt, P. D., Evans, M. J., Edwards, P., Whalley, L. K., Heard, D. E., Slater, E. J., Woodward-Massey, R., Ye, C., Mehra, A., Worrall, S. D., Bacak, A., Coe, H., Percival, C., Hewitt, C. N., Lee, J. D., Cui, T. Q., Surratt, J. D., Wang, X., Lewis, A. C., Rickard, A. R., and Hamilton, J.: Rainforest-like atmospheric chemistry in a polluted megacity, Atmospheric Chemistry and Physics Discussions, 35, 2020.

Peeters, J., Nguyen, T. L., and Vereecken, L.: HOx radical regeneration in the oxidation of isoprene, Phys Chem Chem Phys, 11, 5935-5939, 10.1039/b908511d, 2009.

Peeters, J., Muller, J. F., Stavrakou, T., and Nguyen, V. S.: Hydroxyl Radical Recycling in Isoprene Oxidation Driven by Hydrogen Bonding and Hydrogen Tunneling: The Upgraded LIM1 Mechanism, J Phys Chem A, 118, 8625-8643, 10.1021/jp5033146, 2014.

Reeves, C., Mills, G., Whalley, L. K., Acton, W. J., Bloss, W. J., Crilley, L., Grimmond, C. S. B., Heard, D. E., Hewitt, C. N., Hopkins, J., Kotthaus, S., Kramer, L., Jones, R. L., Lee, J. D., Liu, Y., Ouyang, B., Slater, E. J., Squires, F. A., Wang, X., Woodward-Massey, R., and Ye, C.: Observations of speciated isoprene nitrates in Beijing: Implications for isoprene chemistry, Atmospheric Chemistry and Physics Discussions, 964, 2019.

Ren, X. R., Harder, H., Martinez, M., Lesher, R. L., Oliger, A., Shirley, T., Adams, J., Simpas, J. B., and Brune, W. H.: HOx concentrations and OH reactivity observations in New York City during PMTACS-NY2001, Atmos Environ, 37, 3627-3637, 10.1016/S1352-2310(03)00460-6, 2003.

Ren, X. R., van Duin, D., Cazorla, M., Chen, S., Mao, J. Q., Zhang, L., Brune, W. H., Flynn, J. H., Grossberg, N., Lefer, B. L., Rappengluck, B., Wong, K. W., Tsai, C., Stutz, J., Dibb, J. E., Jobson, B. T., Luke, W. T., and Kelley, P.: Atmospheric oxidation chemistry and ozone production: Results from SHARP 2009 in Houston, Texas, J Geophys Res-Atmos, 118, 5770-5780, 10.1002/jgrd.50342, 2013.

Riedel, T. P., Wolfe, G. M., Danas, K. T., Gilman, J. B., Kuster, W. C., Bon, D. M., Vlasenko, A., Li, S. M., Williams, E. J., Lerner, B. M., Veres, P. R., Roberts, J. M., Holloway, J. S., Lefer, B., Brown, S. S., and Thornton, J. A.: An MCM modeling study of nitryl chloride (ClNO2) impacts on oxidation, ozone production and nitrogen oxide partitioning in polluted continental outflow, Atmos Chem Phys, 14, 3789-3800, 10.5194/acp-14-3789-2014, 2014.

Sadanaga, Y., Yoshino, A., Watanabe, K., Yoshioka, A., Wakazono, Y., Kanaya, Y., and Kajii, Y.: Development of a measurement system of OH reactivity in the atmosphere by using a laser-induced pump and probe technique, Rev Sci Instrum, 75, 2648-2655, 10.1063/1.1775311, 2004.

Saunders, S. M., Jenkin, M. E., Derwent, R. G., and Pilling, M. J.: Protocol for the development of the Master Chemical Mechanism, MCM v3 (Part A): tropospheric degradation of non-aromatic volatile organic compounds, Atmos Chem Phys, 3, 161-180, DOI 10.5194/acp-3-161-2003, 2003.

Shi, Z. B., Vu, T., Kotthaus, S., Harrison, R. M., Grimmond, S., Yue, S., Zhu, T., Lee, J., Han, Y., Demuzere, M., Dunmore, R. E., Ren, L. J., Liu, D., Wang, Y. L., Wild, O., Allan, J., Acton, W. J., Barlow, J., Barratt, B., Beddows, D., Bloss, W. J., Calzolai, G., Carruthers, D., Carslaw, D. C., Chan, Q., Chatzidiakou, L., Chen, Y., Crilley, L., Coe, H., Dai, T., Doherty, R., Duan, F., Fu, P., Ge, B., Ge, M., Guan, D., Hamilton, J. F., He, K., Heal, M., Heard, D., Hewitt, C. N., Hollaway, M., Hu, M., Ji, D., Jiang, X. J., Jones, R., Kalberer, M., Kelly, F. J., Kramer, L., Langford, B., Lin, C., Lewis, A. C., Li, J., Li, W., Liu, H., Liu, J. F., Loh, M., Lu, K. D., Lucarelli, F., Mann, G., McFiggans, G., Miller, M. R., Mills, G., Monk, P., Nemitz, E., O'Connor, F., Bin O. u. y. a. n. g. , Palmer, P. I., Percival, C., Popoola, O., Reeves, C., Rickard, A. R., Shao, L. Y., Shi, G. Y., Spracklen, D., Stevenson, D., Sun, Y., Sun, Z. W., Tao, S., Tong, S. R., Wang, Q. Q., Wang, W. H., Wang, X. M., Wang, X. J., Wang, Z. F., Wei, L. F., Whalley, L., Wu, X. F., Wu, Z. J., Xie, P. H., Yang, F. M., Zhang, Q., Zhang, Y. L., Zhang, Y. H., and Zheng, M.: Introduction to the special issue "In-depth study of air pollution sources and processes within Beijing and its surrounding region (APHH-Beijing)", Atmos Chem Phys, 19, 7519-7546, 10.5194/acp-19-7519-2019, 2019.

Slater, E. J., Whalley, L. K., Woodward-Massey, R., Ye, C., Lee, J. D., Squires, F. A., Hopkins, J., Dunmore, R., Shaw, M., Hamilton, J. F., Lewis, A. C., Crilley, L., Kramer, L., Bloss, W. J., Vu, T., Sun, Y., Xu, W., Yue, S., Ren, L., Acton, W. J., Hewitt, C. N., Wang, X., Fu, P., and Heard, D. E.: Elevated levels of OH observed in haze events during wintertime in central Beijing, Atmospheric Chemistry and Physics Discussions, 362, 2020.

Squires, F. A., Nemitz, E., Langford, B., Wild, O., Drysdale, W. S., Acton, W. J., Fu, P., Grimmond, C. S. B., Hamilton, J. F., Hewitt, C. N., Hollaway, M., Kotthaus, S., Lee, J., Metzger, S., Pingintha-Durden, N., Shaw, M., Vaughan, A. R., Wang, X., Wu, R., Zhang, Q., and Zhang, Y.: Measurements of traffic-dominated pollutant emissions in a Chinese megacity, Atmos Chem Phys, 20, 8737-8761, 2020.

Tan, Z. F., Fuchs, H., Lu, K. D., Hofzumahaus, A., Bohn, B., Broch, S., Dong, H. B., Gomm, S., Haseler, R., He, L. Y., Holland, F., Li, X., Liu, Y., Lu, S. H., Rohrer, F., Shao, M., Wang, B. L., Wang, M., Wu, Y. S., Zeng, L. M., Zhang, Y. S., Wahner, A., and Zhang, Y. H.: Radical chemistry at a rural site (Wangdu) in the North China Plain: observation and model calculations of OH, HO2 and RO2 radicals, Atmos Chem Phys, 17, 663-690, 10.5194/acp-17-663-2017, 2017.

Tan, Z. F., Lu, K. D., Hofzumahaus, A., Fuchs, H., Bohn, B., Holland, F., Liu, Y. H., Rohrer, F., Shao, M., Sun, K., Wu, Y. S., Zeng, L. M., Zhang, Y. S., Zou, Q., Kiendler-Scharr, A., Wahner, A., and Zhang, Y. H.: Experimental budgets of OH, HO2, and RO2 radicals and implications for ozone formation in the Pearl River Delta in China 2014, Atmos Chem Phys, 19, 7129-7150, 10.5194/acp-19-7129-2019, 2019.

Tan, Z. F., Hofzumahaus, A., Lu, K. D., Brown, S. S., Holland, F., Huey, L. G., Kiendler-Scharr, A., Li, X., Liu, X. X., Ma, N., Min, K. E., Rohrer, F., Shao, M., Wahner, A., Wang, Y. H., Wiedensohler, A., Wu, Y. S., Wu, Z. J., Zeng, L. M., Zhang, Y. H., and Fuchs, H.: No Evidence for a Significant Impact of Heterogeneous Chemistry on Radical Concentrations in the North China Plain in Summer 2014, Environ Sci Technol, 54, 5973-5979, 10.1021/acs.est.0c00525, 2020.

Wang, S. N., Wu, R. R., Berndt, T., Ehn, M., and Wang, L. M.: Formation of Highly Oxidized Radicals and Multifunctional Products from the Atmospheric Oxidation of Alkylbenzenes, Environ Sci Technol, 51, 8442-8449, 10.1021/acs.est.7b02374, 2017b.

Wang, T., Ding, A. J., Gao, J., and Wu, W. S.: Strong ozone production in urban plumes from Beijing, China, Geophys Res Lett, 33, Artn L21806 10.1029/2006gl027689, 2006.

Wang, T., Nie, W., Gao, J., Xue, L. K., Gao, X. M., Wang, X. F., Qiu, J., Poon, C. N., Meinardi, S., Blake, D., Wang, S. L., Ding, A. J., Chai, F. H., Zhang, Q. Z., and Wang, W. X.: Air quality during the 2008 Beijing Olympics: secondary pollutants and regional impact, Atmos Chem Phys, 10, 7603-7615, 10.5194/acp-10-7603-2010, 2010.

Wang, T., Xue, L. K., Brimblecombe, P., Lam, Y. F., Li, L., and Zhang, L.: Ozone pollution in China: A review of concentrations, meteorological influences, chemical precursors, and effects, Sci Total Environ, 575, 1582-1596, 10.1016/j.scitotenv.2016.10.081, 2017a.

Whalley, L. K., Edwards, P. M., Furneaux, K. L., Goddard, A., Ingham, T., Evans, M. J., Stone, D., Hopkins, J. R., Jones, C. E., Karunaharan, A., Lee, J. D., Lewis, A. C., Monks, P. S., Moller, S. J., and Heard, D. E.: Quantifying the magnitude of a missing hydroxyl radical source in a tropical rainforest, Atmos Chem Phys, 11, 7223-7233, 10.5194/acp-11-7223-2011, 2011.

Whalley, L. K., Blitz, M. A., Desservettaz, M., Seakins, P. W., and Heard, D. E.: Reporting the sensitivity of laser-induced fluorescence instruments used for HO2 detection to an interference from RO2 radicals and introducing a novel approach that enables HO2 and certain RO2 types to be selectively measured, Atmos Meas Tech, 6, 3425-3440, 10.5194/amt-6-3425-2013, 2013.

Whalley, L. K., Stone, D., Bandy, B., Dunmore, R., Hamilton, J. F., Hopkins, J., Lee, J. D., Lewis, A. C., and Heard, D. E.: Atmospheric OH reactivity in central London: observations, model predictions and estimates of in situ ozone production, Atmos Chem Phys, 16, 2109-2122, 10.5194/acp-16-2109-2016, 2016.

Whalley, L. K., Stone, D., Dunmore, R., Hamilton, J., Hopkins, J. R., Lee, J. D., Lewis, A. C., Williams, P., Kleffmann, J., Laufs, S., Woodward-Massey, R., and Heard, D. E.: Understanding in situ ozone production in the summertime through radical observations and modelling studies during the Clean air for London project (ClearfLo), Atmos Chem Phys, 18, 2547-2571, 10.5194/acp-18-2547-2018, 2018.

Woodward-Massey, R., Slater, E. J., Alen, J., Ingham, T., Cryer, D. R., Stimpson, L. M., Ye, C. X., Seakins, P. W., Whalley, L. K., and Heard, D. E.: Implementation of a chemical background method for atmospheric OH measurements by laser-induced fluorescence: characterisation and observations from the UK and China, Atmos Meas Tech, 13, 3119-3146, 10.5194/amt-13-3119-2020, 2020.

Xue, L. K., Saunders, S. M., Wang, T., Gao, R., Wang, X. F., Zhang, Q. Z., and Wang, W. X.: Development of a chlorine chemistry module for the Master Chemical Mechanism, Geosci Model Dev, 8, 3151-3162, 10.5194/gmd-8-3151-2015, 2015.

Zhou, W., Zhao, J., Ouyang, B., Mehra, A., Xu, W. Q., Wang, Y. Y., Bannan, T. J., Worrall, S. D., Priestley, M., Bacak, A., Chen, Q., Xie, C. H., Wang, Q. Q., Wang, J. F., Du, W., Zhang, Y. J., Ge, X. L., Ye, P. L., Lee, J. D., Fu, P. Q., Wang, Z. F., Worsnop, D., Jones, R., Percival, C. J., Coe, H., and Sun, Y. L.: Production of N2O5 and ClNO2 in summer in urban Beijing, China, Atmos Chem Phys, 18, 11581-11597, 10.5194/acp-18-11581-2018, 2018.

Table 1: Chemical reactions that were used in the experimental budget analysis for OH, HO_2, RO_2 and RO_x. The rate coefficient at 298K are given in column 3; temperature dependent rate coefficients were used in the experimental budget analysis presented in section 3.3

No.	**Reaction**	**Rate coefficient (298K) cm^3 $molecule^{-1}$ s^{-1}**
R1	$\text{Alkene} + O_3 \rightarrow OH, HO_2, RO_2 + \text{products}$	Specific rate coefficients and radical yields for each alkene, taken from the MCM3.3.1 (Jenkin et al., 2015)
R2	$NO + HO_2 \rightarrow OH + NO$	8.5×10^{-12}
R3	$O_3 + HO_2 \rightarrow OH + 2O_2$	2.0×10^{-15}
R4	$HCHO + OH + O_2 \rightarrow CO + HO_2 + H_2O$	8.4×10^{-12}
R5	$CO + OH + O_2 \rightarrow HO_2 + CO_2$	2.3×10^{-13}
R6	$RO_2 + NO \rightarrow RO + NO_2$	8.7×10^{-12}
R7	$HO_2 + NO \rightarrow OH + NO_2$	8.5×10^{-12}
R8	$HO_2 + O_3 \rightarrow OH + 2O_2$	2.0×10^{-15}
R9	$HO_2 + RO_2 \rightarrow ROOH + O_2$	2.3×10^{-11}
R10	$HO_2 + HO_2 \rightarrow H_2O_2 + O_2$ $HO_2 + HO_2 + H_2O \rightarrow H_2O_2 + H_2O + O_2$	1.7×10^{-12} 6.4×10^{-30}
R11	$RO_2 + RO_2 \rightarrow \text{products}$	3.5×10^{-13}
R12	$OH + NO_2 \rightarrow HNO_3$	1.1×10^{-11}
R13	$OH + NO \rightarrow HONO$	7.5×10^{-12}

Table 2: The species measured by DC-GC-FID and PTR-ToF-MS that have been used as constraints in the model

Instrument	Species	Reference
DC-GC_FID	CH_4, C_2H_6, C_2H_4, C_3H_8, C_3H_6, isobutane, butane, C_2H_2, trans-but-2-ene, but-1ene, Isobutene, cis-but-2-ene, 2-Methylbutane, pentane, 1,3-butadiene, trans-2-pentene, cis-2-pentene, 2-methylpetane, 3-methypetane, hexane, isoprene, heptane, Benzene, Toluene, o-xylene, CH_3OH, CH_3OCH_3, ethylbenzene, CH_3CHO, C_2H_5OH	Hopkins et al. (2011)
PTR-ToF-MS	α-pinene, limonene, isopropylbenzene, propylbenzene, xylene, trimethylbenzene.	Huang et al. (2016)

930

Table 3: Different model scenarios that are discussed in section 3

Model Name	**Description**
Base model	As described in section 2.4
Base model-SA	The base model with the inclusion of a first order loss process of HO_2 to aerosols calculated using Eq 9 with an uptake coefficient, $\gamma = 0.2$
Base model-Cl	The base model with the inclusion of Cl atom chemistry, taken from (Xue et al., 2015)
Missing k(OH) (OH to CH_3O_2)	The base model with an additional reaction converting OH to CH_3O_2 at a rate equal to the missing reactivity
Missing k(OH) (OH to $HOCH_2CH_2O_2$)	The base model with an additional reaction converting OH to $HOCH_2CH_2O_2$ at a rate equal to the missing reactivity
Missing k(OH) (OH to $CH_3C(O)O_2$)	The base model with an additional reaction converting OH to $CH_3C(O)O_2$ at a rate equal to the missing reactivity
Missing k(OH) (OH to C96O2)[1] **C96O2 =** 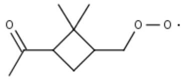	The base model with an additional reaction converting OH to C96O2 (which is an α-pinene derived RO_2 species) at a rate equal to the missing reactivity

[1] Note, C96O2 is an α-pinene derived RO_2 that forms during the ozone-initiated oxidation of α-pinene. The additional production of C96O2 peroxy radicals in this model scenario was used to investigate the impact of an RO isomerisation mechanism on the modelled radical concentrations.

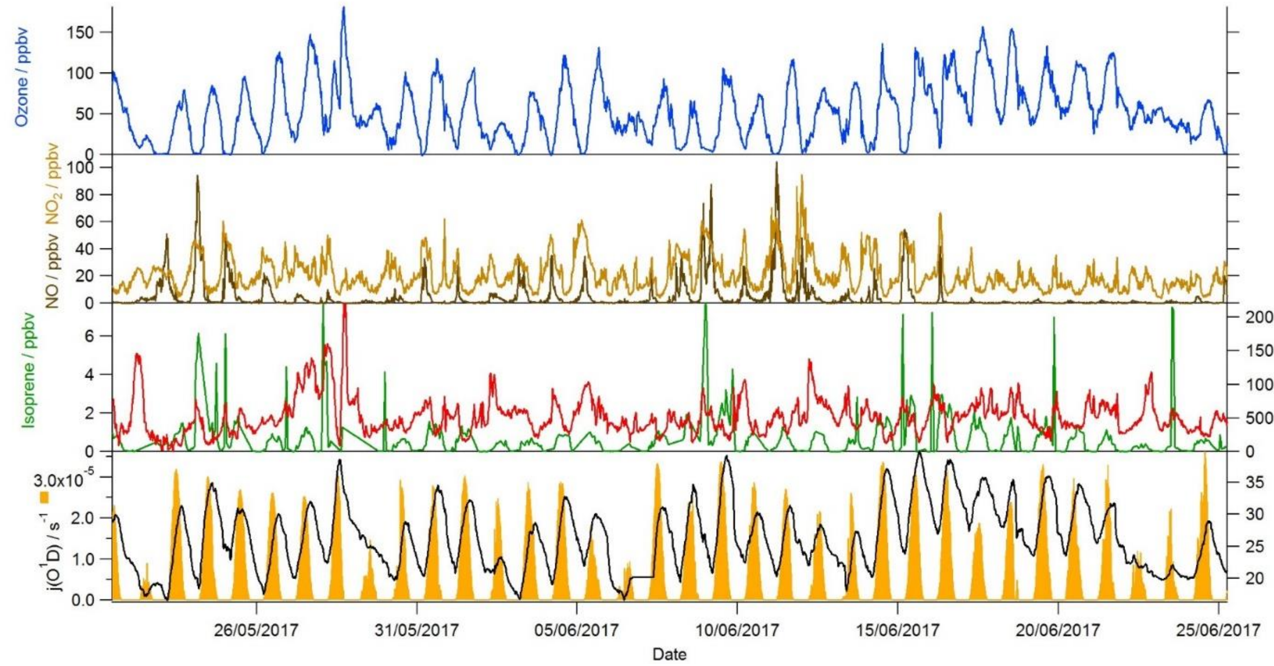

Figure 1: Time-series of ozone, NO, NO$_2$ isoprene, CO, j(O^{1}D) and temperature during the campaign

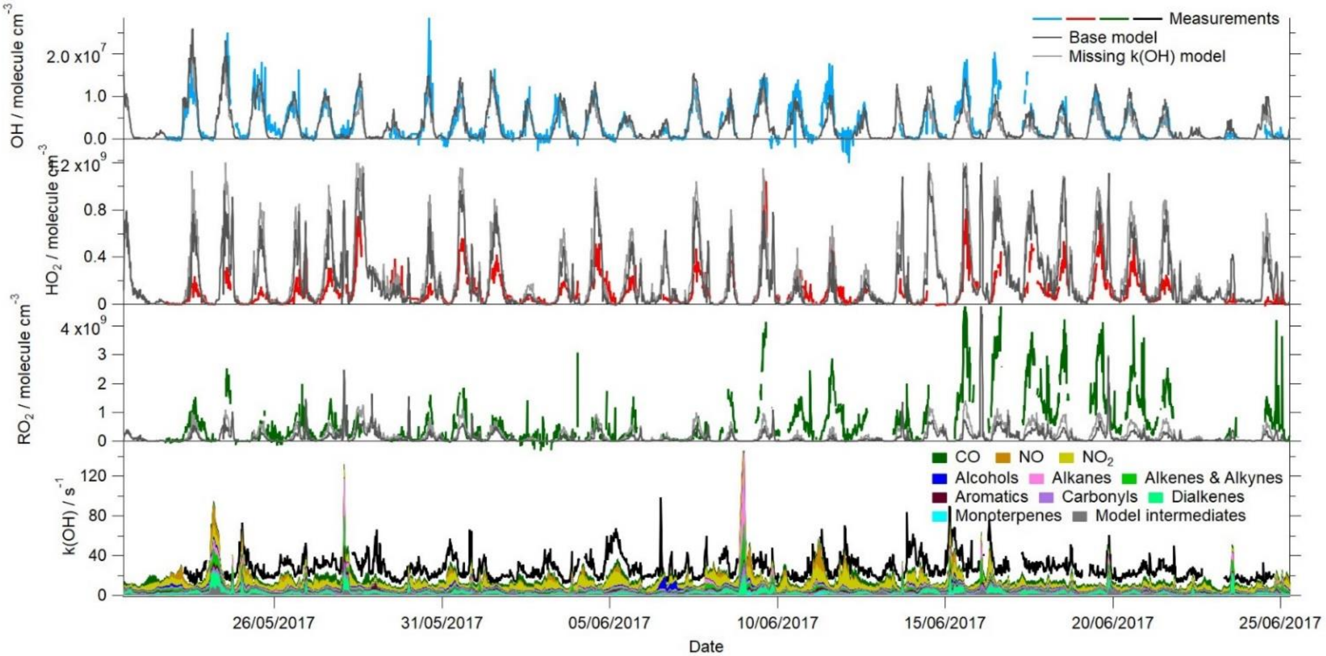

Figure 2: Time-series of the measured and modelled OH, HO$_2$, total RO$_2$ and OH reactivity during the campaign

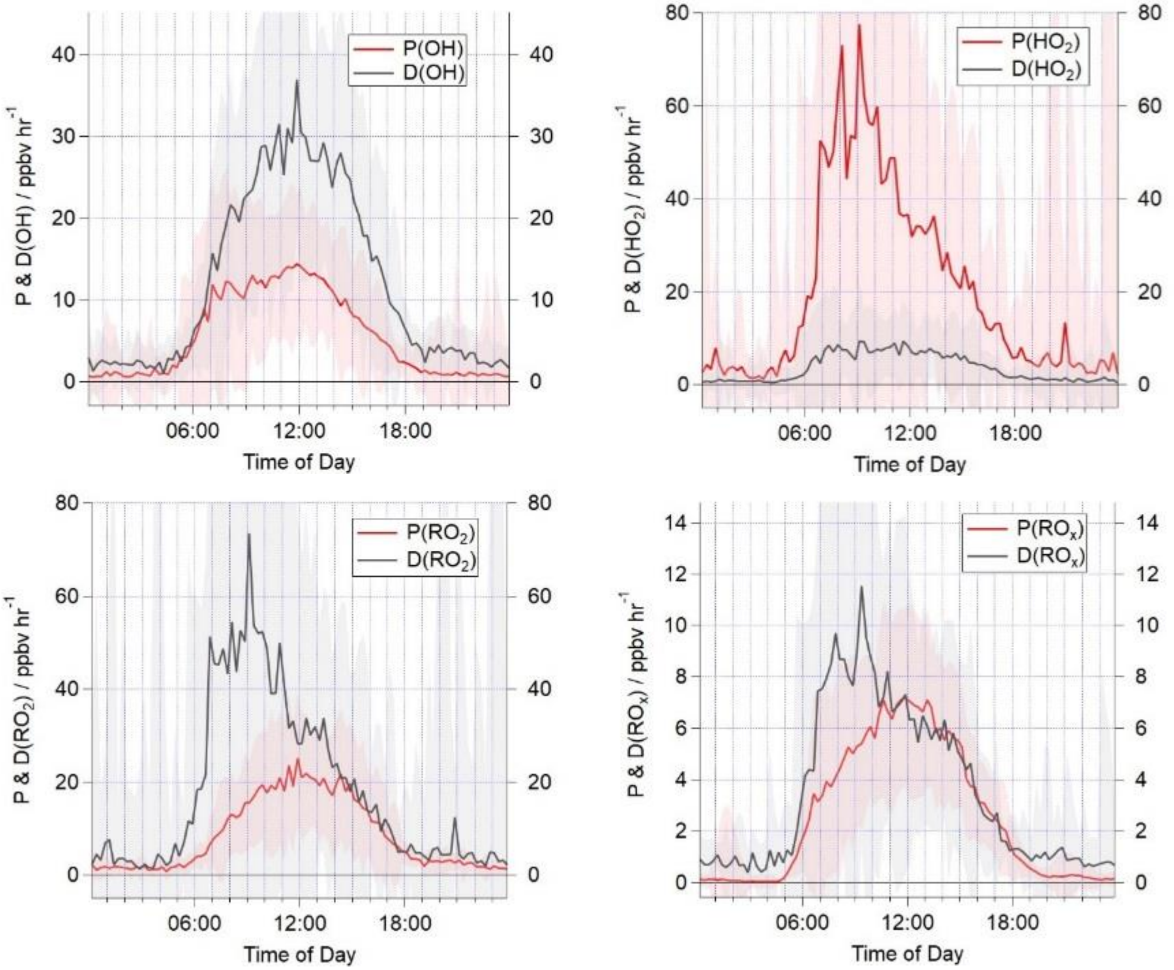

Figure 3: Campaign median production and destruction rates for OH, HO_2, total RO_2 and RO_x. The shaded areas represent the 1σ standard deviation of the data representing the variability from day to day

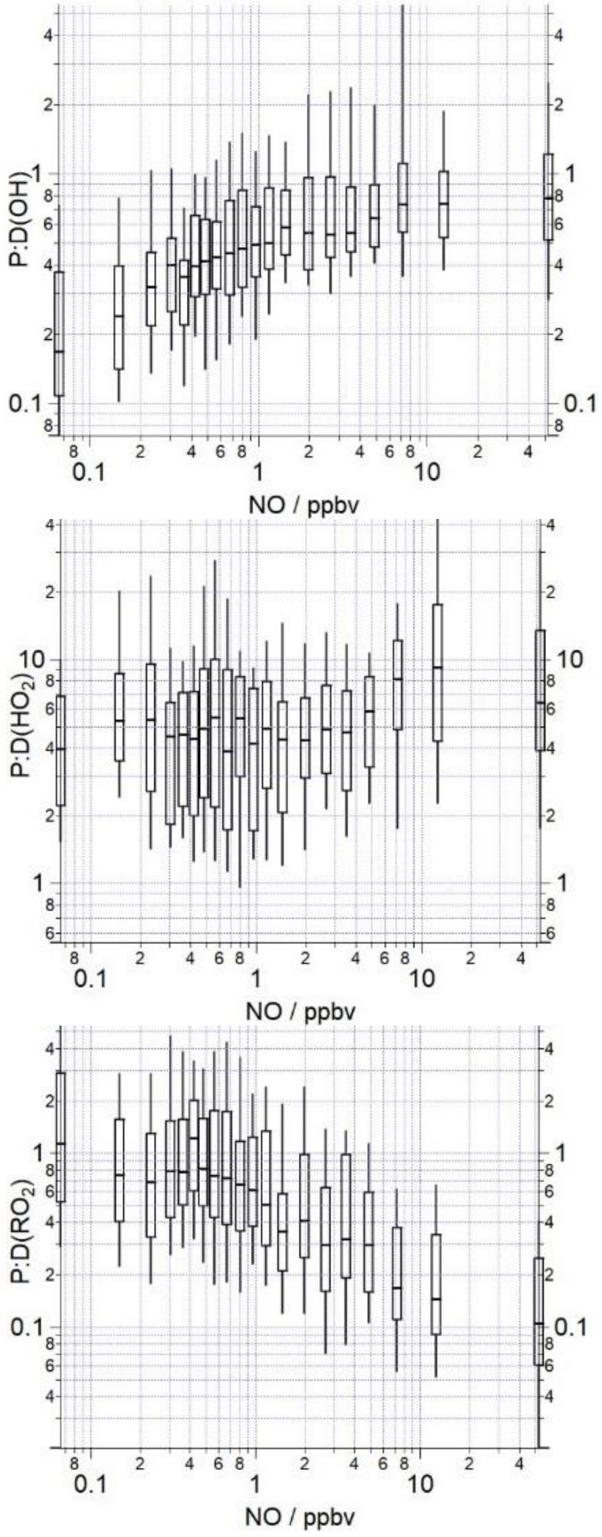

Figure 4: The median ratio of the OH, HO_2 and total RO_2 production rates to destruction rates binned over the NO mixing ratio range encountered during the campaign on a logarithmic scale. The box and whiskers represent the 25th/75th and 5th/95th confidence intervals. The number of data points in each of the NO bins is ~80

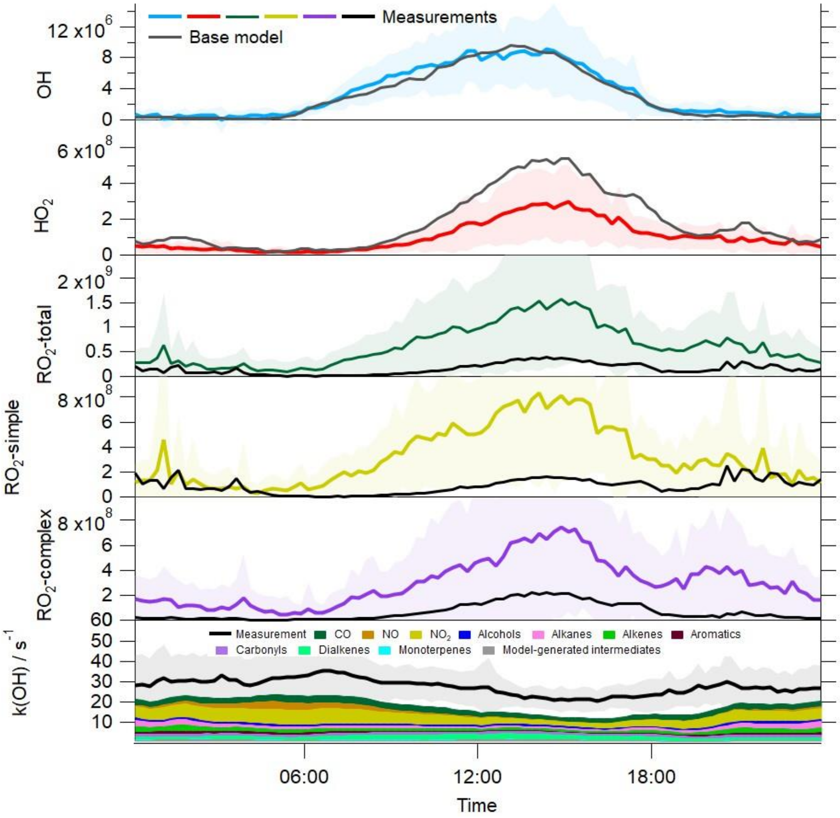

Figure 5: Average profiles for the observed OH, HO$_2$, total RO$_2$, partially-speciated RO$_2$ (in molecule cm^{-3}) and OH reactivity at 15 minute intervals over 24 hours. The error bars represent the 1 σ standard deviation of the measurements representing the variability in the measurements from day to day. The average diurnal profiles for OH, HO$_2$, total RO$_2$, partially speciated RO$_2$ and OH reactivity from the base model are overlaid

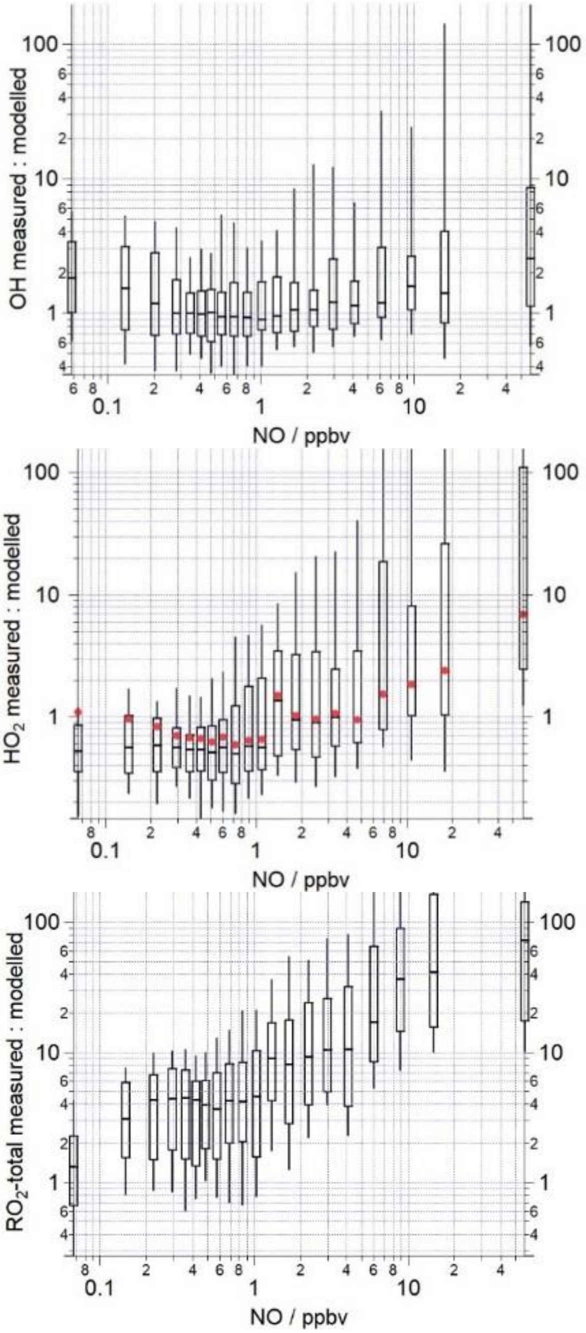

Figure 6: The median ratio (-) of the measured to modelled OH, HO$_2$ and total RO$_2$ binned over the NO mixing ratio range encountered during the campaign on a logarithmic scale. The box and whiskers represent the 25th/75th and 5th/95th confidence intervals. The red circles in the middle panel display the measured to modelled HO$_2$ ratio when the model includes a heterogeneous loss of HO$_2$ to aerosols calculated using Eq. 9. The number of data points in each of the NO bins is ~80

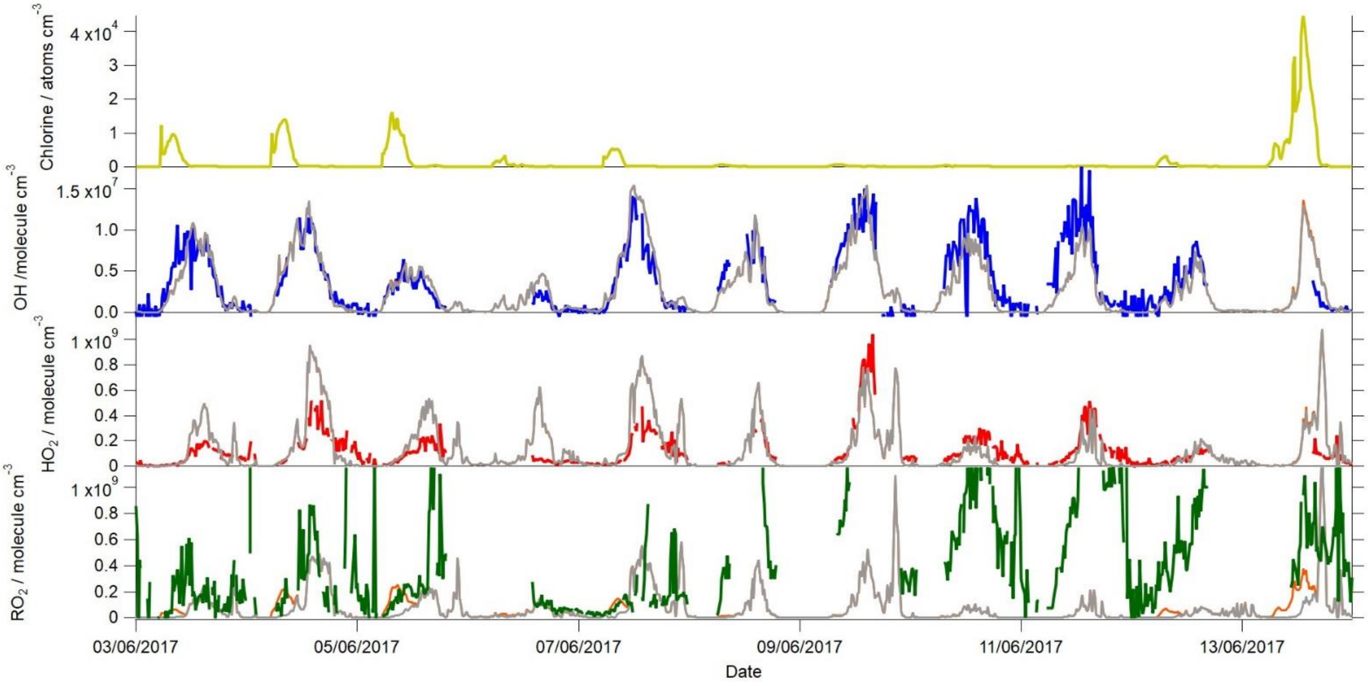

Figure 7: Time-series of the measured and modelled OH, HO_2, total RO_2 during the campaign when $ClNO_2$ was also measured. The Cl atom concentration calculated to be present is shown in the top panel. The measured OH concentrations are represented by the blue line, HO_2 by the red line and total RO_2 by the green line. The base model scenario is shown in grey, whilst the base model with Cl atom chemistry included (Xue et al., 2015) is shown in orange 1090

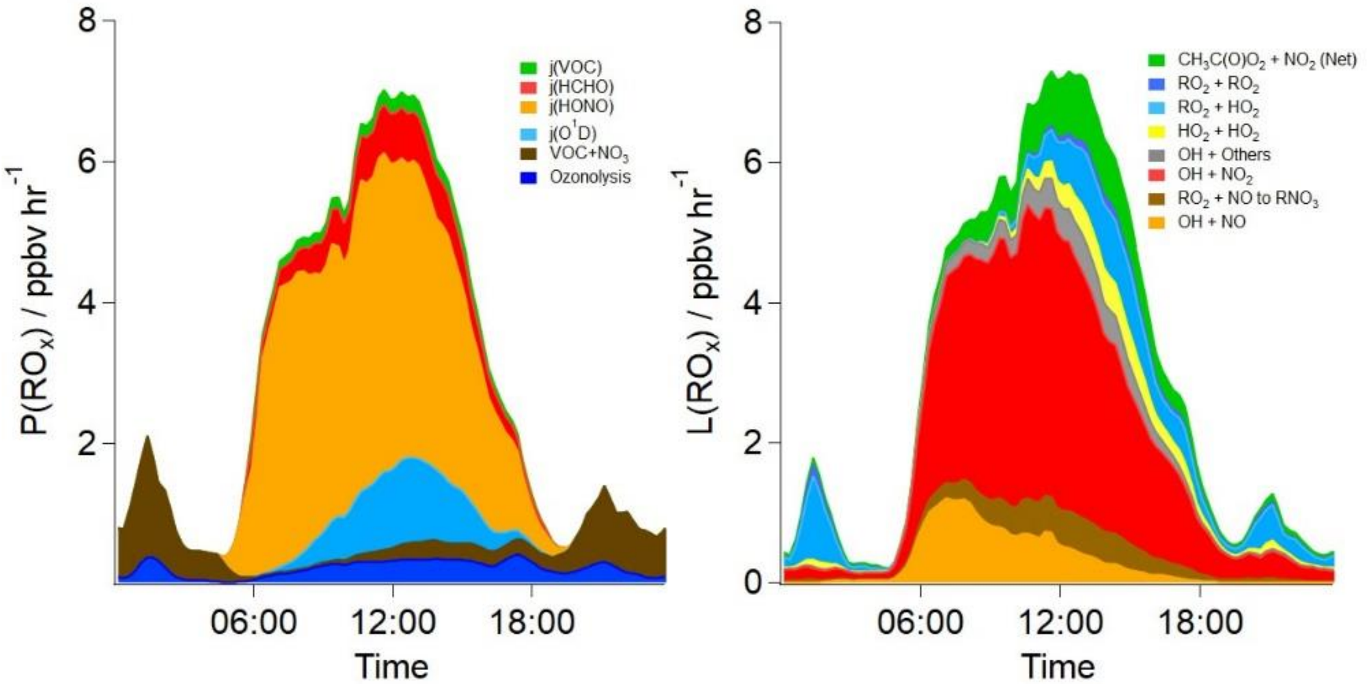

Figure 8: The average diurnal rates of primary production and termination for RO$_x$ radicals in ppbv hr^{-1} in the base model scenario. CH$_3$C(O)O$_2$+ NO$_2$ (Net) represents the net rate (forward minus backward) for all RC(O)O$_2$+ NO$_2$ ↔ PAN species

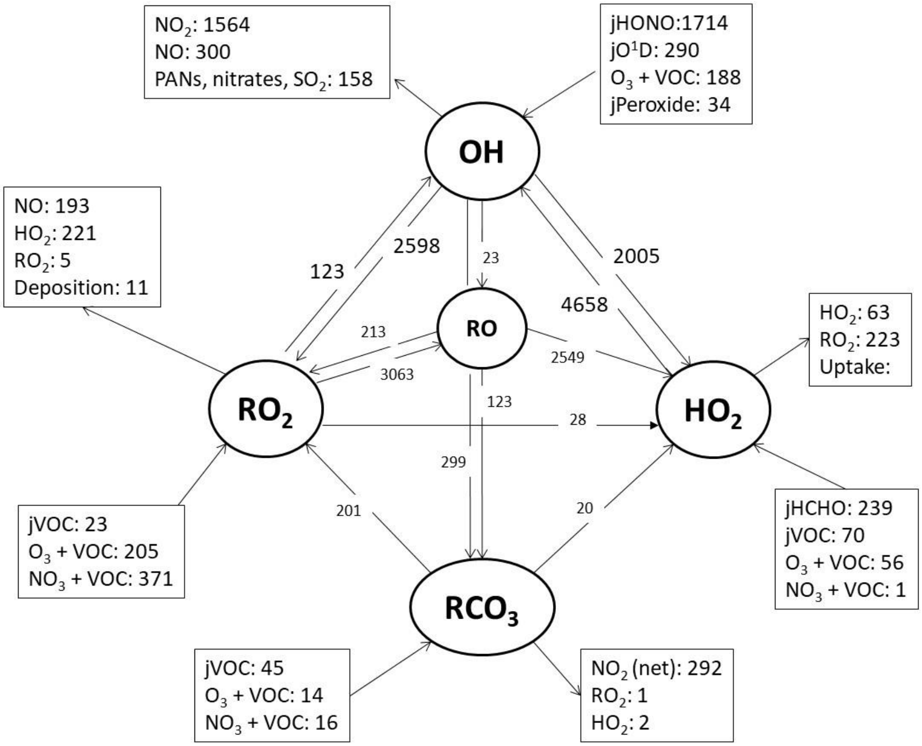

Figure 9: A model reaction flux analysis, showing the mean rate of reaction for formation, propagation and termination of radicals (pptv hr^{-1}) (day and night) during the whole campaign

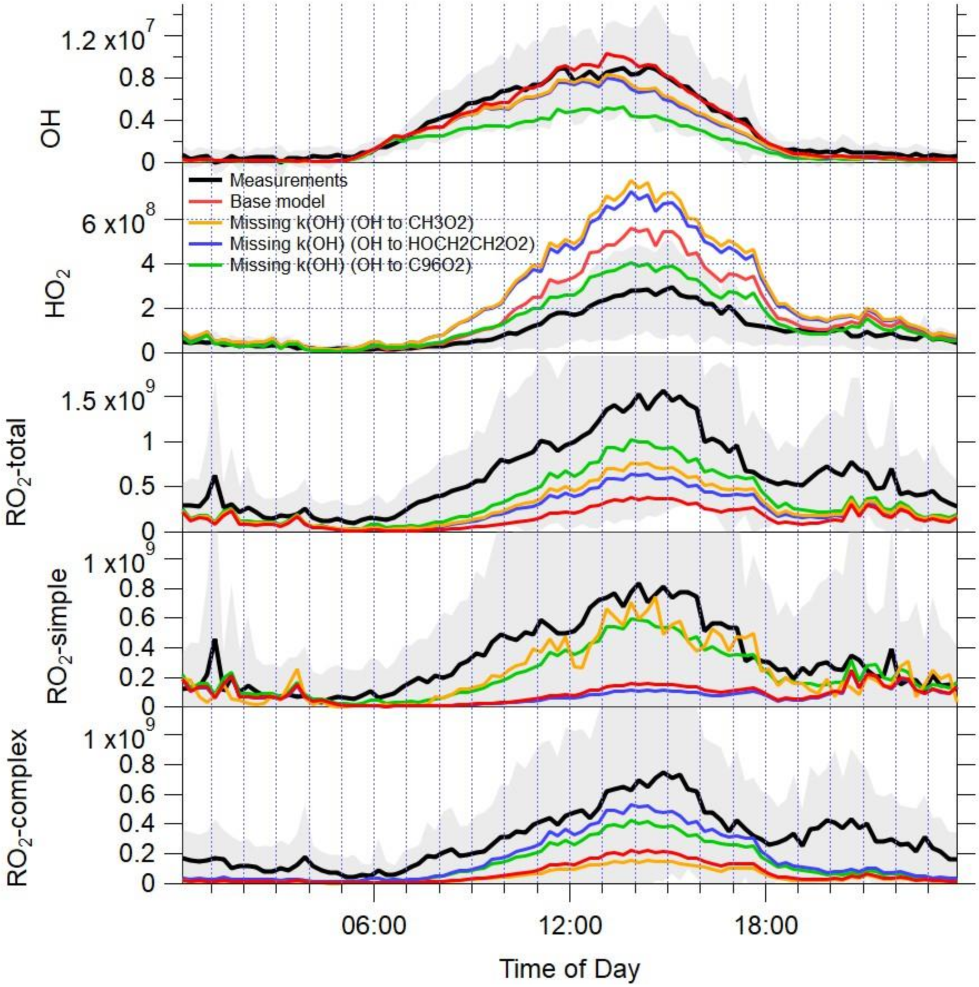

Figure 10: Average diel profiles for the observed OH, HO_2, total RO_2, and partially-speciated RO_2 (black lines) at 15 minute intervals over 24 hours. The error bars represent the 1 σ standard deviation of the measurements. The average OH, HO_2, total RO_2 and partially speciated RO_2 model profiles when the missing reactivity observed at a given time is accounted for by different OH to RO_2 reactions are overlaid (yellow, blue and green lines); the base model predictions are in red. See text for details 1105

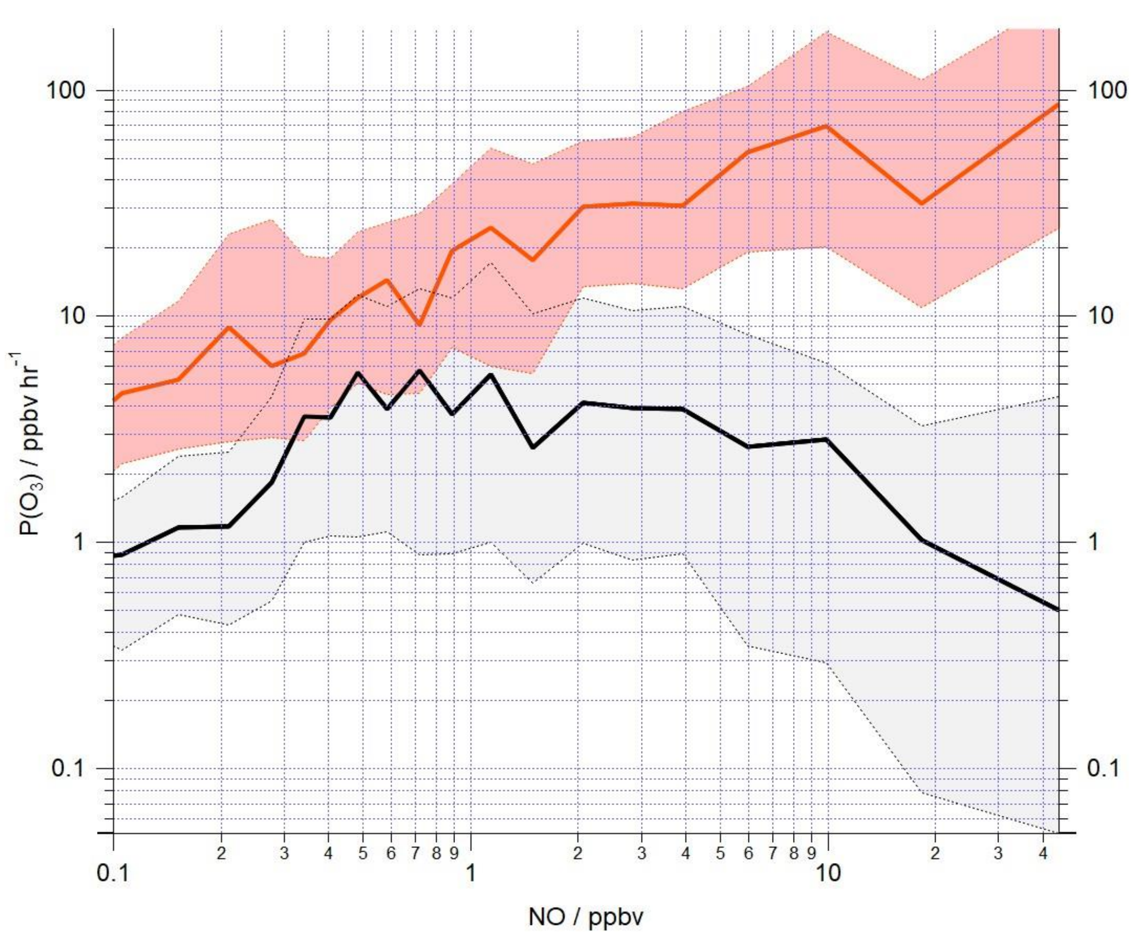

1110

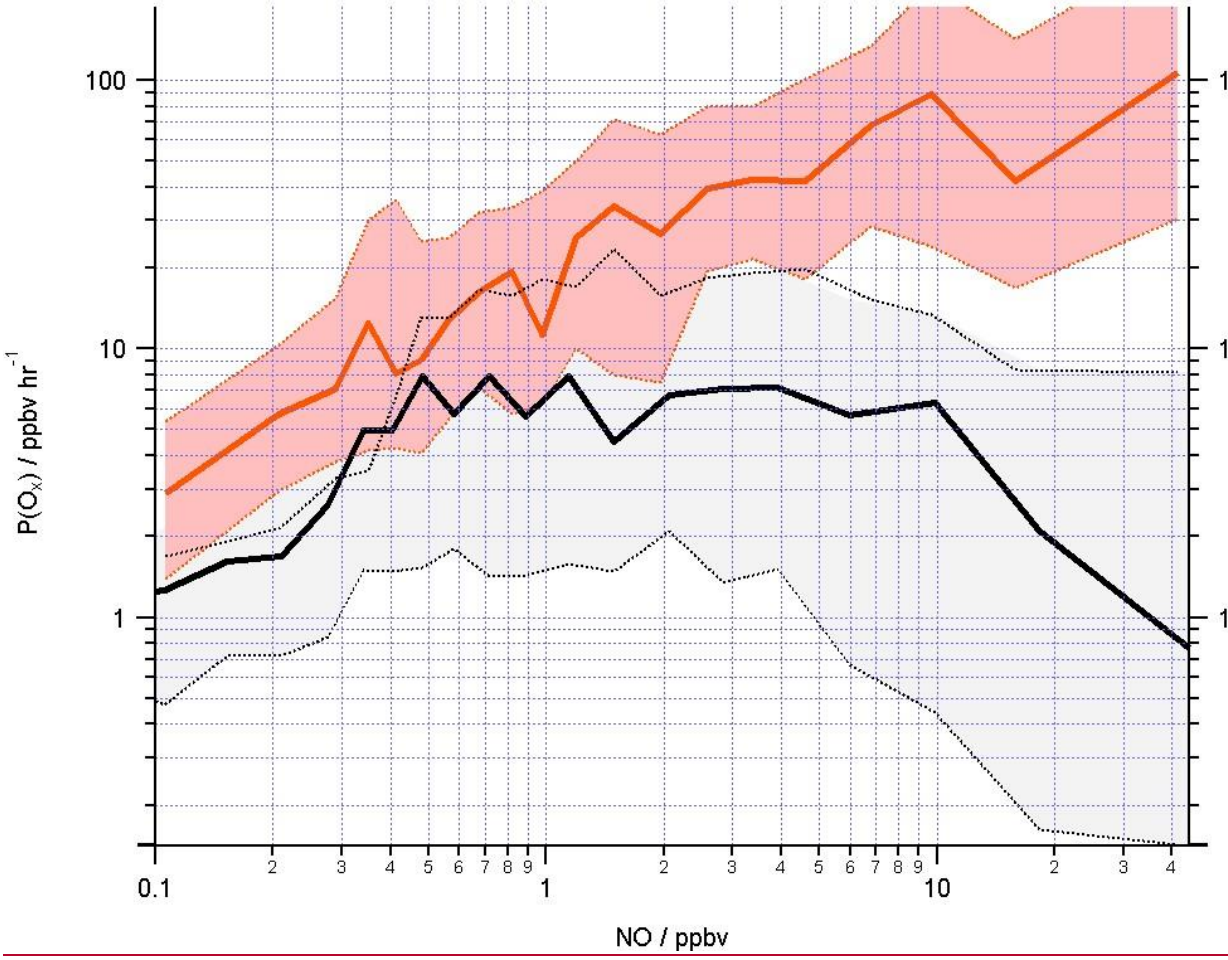

Figure 11: Mean ~~ozone~~ O_x production (ppbv hr^{-1}) calculated from observed (red line) and modelled (black line) RO_x concentrations using Eq. (11) binned over the NO mixing ratio range encountered during the campaign on a logarithmic scale. The shading represents the 25th / 75th percentile confidence limits. The number of data points in each of the NO bins is ~80